Channel-Training-Aided Target Sensing for Terahertz Integrated Sensing and Massive MIMO Communications

Ruoyu Zhang, *Member, IEEE*, Xiaopeng Wu, Yi Lou, *Member, IEEE*, Feng-Gang Yan, Zhiquan Zhou, Wen Wu, *Senior Member, IEEE*, and Chau Yuen, *Fellow, IEEE*

***Abstract*—Integrated sensing and massive multiple-input–multiple-output (MIMO) communication (mMIMO-ISAC) at terahertz (THz) bands can provide vast spatial degrees of freedom and abundant bandwidth resources. However, the employment of a massive number of antennas will pose prominent challenges to both target sensing and channel training in THz-mMIMO-ISAC. In this article, our goal is to integrate the target sensing functionality into the channel estimation stage and develop a channel-training-aided target sensing framework to facilitate the efficient resource sharing of THz-mMIMO-ISAC. Specifically, by exploiting the sparse characteristics of THz mMIMO channels, we build up the intrinsic connection between the channel parameters and the target parameters in angular, delay, and Doppler dimensions. Then, we propose a shared channel training pattern accommodating the hybrid architecture constraints of THz transceiver. Both the channel estimation and the target sensing can be formulated as two structured tensor decomposition problems and then concurrently addressed at the UE and BS sides, respectively. Next, we propose a tensor-based parameter estimation algorithm to acquire the target and channel parameters, where the associated angles of arrival/departure, time delays, Doppler shifts, and coefficients can be extracted from the estimated factor matrices. In addition, we present the detailed derivation of the Cramér–Rao bound (CRB) for the considered parameter estimation problem in THz-mMIMO-ISAC. Numerical results demonstrate that the proposed algorithm can achieve the target parameters estimation performance close to their corresponding CRB, and recover the high-dimensional THz mMIMO channels with substantially reduced training overhead.**

***Index Terms*—Channel estimation and target sensing, hybrid architectures, integrated sensing and communication (ISAC), tensor decomposition, terahertz (THz) massive multiple-input–multiple-output (mMIMO).**

Manuscript received 13 March 2024; revised 20 July 2024; accepted 18 August 2024. Date of publication 23 August 2024; date of current version 6 February 2025. This work was supported in part by the National Natural Science Foundation of China under Grant 62201266, Grant 62171150, and Grant 62101152; in part by the Natural Science Foundation of Jiangsu Province under Grant BK20210335; and in part by the Taishan Scholar Project of Shandong Province of China under Grant tsqn202211087 and Grant tsqn202312142. *(Corresponding author: Yi Lou.)*

Ruoyu Zhang, Xiaopeng Wu, and Wen Wu are with the Key Laboratory of Near-Range RF Sensing ICs and Microsystems (NJUST), Ministry of Education, School of Electronic and Optical Engineering, Nanjing University of Science and Technology, Nanjing 210094, China (e-mail: ryzhang19@njust.edu.cn; xpwu@njust.edu.cn; wuwen@njust.edu.cn).

Yi Lou, Feng-Gang Yan, and Zhiquan Zhou are with the School of Information Science and Engineering, Harbin Institute of Technology (Weihai), Weihai 264209, China (e-mail: louyi@ieee.org; yfglion@163.com; zzq@hitwh.edu.cn).

Chau Yuen is with the School of Electrical and Electronics Engineering, Nanyang Technological University, Singapore 639798 (e-mail: chau.yuen@ntu.edu.sg).

Digital Object Identifier 10.1109/JIOT.2024.3447584

I. Introduction

SENSING is anticipated to play an indispensable role in future sixth-generation (6G) wireless networks to support emerging scenarios, such as smart home, Industry 4.0, and smart cities in Internet of Everything (IoE) [1], [2], [3]. These scenarios not only require high data rate transmission for communications but also demand high-resolution and accurate sensing ability, which promotes the promising technology of integrated sensing and communication (ISAC) [4], [5], [6]. Terahertz (THz) bands, owing to its vast spectrum resources, are potential to significantly boost both the communication and sensing performance of ISAC [7]. Massive multiple-input–multiple-output (mMIMO) [8], [9], as a representative technology for 5G and future 6G, can not only produce the considerable array gain to compensate the severe propagation attenuation in THz bands but also enhance the spatial resolution for sensing and system capacity for communication. It is foreseeable that the combination of ISAC with mMIMO at THz bands (THz-mMIMO-ISAC) can provide ultrabroad bandwidth and abundant spatial degrees of freedom, making it possible to enable ultrafast communication transmission and ultrahigh-resolution target sensing [10], [11], [12].

Despite the immense potentials, the employment of a massive number of antennas will pose significant signal processing challenges to both sensing and communication functionalities in THz-mMIMO-ISAC. To be specific, the large number of antennas at both the transmitter and receiver will not only introduce high power consumption of hardware implementation but also induce a significant computational burden on sensing the unknown parameters associated with the targets. This issue becomes more pronounced when considering the low efficiency of THz hardware components and the round-trip signal propagation of the target sensing. Besides, a large number of unknown coefficients in high-dimensional communication channel matrix requires excessive pilot overhead. Considering the more obvious Doppler effect in THz bands, the more frequent channel training will further deteriorate the communication spectral efficiency [13], [14]. Given these

critical issues, it is necessary to investigate the effective target sensing and channel training methods for THz-mMIMO-ISAC.

As a core task in radar systems, target sensing has been independently studied over the past decades [15], [16], [17] and is attracting increasing attention in ISAC systems in recent years [18], [19], [20], [21], [22], [23], [24], [25], [26]. For instance, the recent work in [20] exploited the orthogonal frequency-division multiplexing (OFDM) signals to estimate the delay, Doppler, and angle parameters of multiple targets in millimeter-wave (mmWave) MIMO-ISAC systems. Also, Zhang et al. [25] investigated the dual-functional constant modulus waveform design for simultaneously transmitting and reconfigurable intelligent surface-aided ISAC. To fulfill the efficient target sensing in THz ISAC, Mao et al. [27] designed the waveform with multisubband quasi-perfect sequences to alleviate the sampling rate requirement. Also, Wu et al. [28] proposed a sensing integrated discrete Fourier transform spread OFDM signal, which can adapt to the flexible delay spread of THz channels with lower peak-to-average power ratio. As the number of antenna becomes massive, however, the hardware cost and power consumption of THz mMIMO with fully digital architectures, i.e., each antenna connects to one dedicated radio-frequency (RF) chain, is prohibitively unbearable [29]. To reduce the hardware complexity, the concept of phased-MIMO radar, from the field of radar, was proposed in [30], which can strike a favorable performance tradeoff between phased-array and MIMO radars. The similar concept has also emerged in the field of communication, namely, hybrid analog–digital (HAD) architecture, which is treated as an appealing means to realize the tradeoff between the implementation complexity and the system performance in mmWave/THz communication [31], [32]. Given the natural connections of these hybrid architectures, Cheng et al. [33] proposed an alternating optimization-based HAD beamforming design scheme for OFDM-based MIMO-ISAC systems. Zhang et al. [34] developed a dynamic maximum likelihood direction-of-arrival estimation method for different hybrid architectures. Recently, Gao et al. [35] proposed a novel scheme for sensing user directions by exploiting the beam-squint effect of THz mMIMO. Nevertheless, the reduced number of RF chains in these hybrid architectures significantly decreases the dimension of the received signals, consuming a large amount of time–frequency resources for acquiring the high-dimensional channel in THz-mMIMO-ISAC.

From the perspective of communications, efficient channel training is essential for achieving the communication capacity and the potential performance gains of mMIMO. Previous work in mMIMO communication systems mainly focuses on the mmWave band, where the channel sparsity in either the angular domain [36], [37], [38] or the delay domain [39], [40], [41], has been fully exploited to reduce the channel training overhead under the framework of compressive sensing (CS). As a further step, recent research works leveraged the tensor-based signal processing technique for mMIMO channel estimation [42], [43], [44], [45], [46], where the multidimensional parameters (i.e., angles, time delays, or Doppler shifts) of each mmWave channel path can be accurately estimated. As the carrier frequency further goes up to THz band, it has been shown that the signal loss caused by scattering, diffraction, and blockage, etc., is more substantial, resulting the Line-of-Sight (LoS)-dominant propagation and even sparse channels [13], [47]. By exploiting this peculiarity, Wan et al. [48] developed an effective closed-loop broadband channel estimation scheme by leveraging both the angular- and delay-domain sparsity of THz mMIMO channels. To deal with the fast variation of THz channels under the user mobility scenarios, Gao et al. [49] proposed a priori-aided channel tracking scheme by taking the temporal correlation of the angular channels into account, which alleviates the unaffordable pilot overhead. In the case of wide signal bandwidths along with large array aperture, Dovelos et al. [50] formulated a sparse representation of the THz channel and transformed the channel estimation into a CS problem, where a wideband dictionary capturing the common support of channels across different OFDM subcarriers was employed. Although these methods are effective to alleviate the training overhead for channel estimation, the aforementioned works specifically concentrated on THz mMIMO communications, and may not be straightforwardly suitable for ISAC scenarios.

It is noticeable that the aforementioned channel estimation process is similar to the sensing process, which essentially acquires the unknown target parameters by transmitting a known probing signal [51], [52]. A natural thought is to consider whether we can exploit the target sensing process for channel acquisition or vice versa. Following this spirit, Liu et al. [53] proposed to utilize the echo signals of vehicle targets for predictive beamforming design, which eliminates the need for feedback loop and reduces the signaling overhead for beam-tracking. Also, a MIMO radar-aided channel estimation scheme was proposed to reduce the training overhead in vehicle-to-everything scenarios [54]. Gao et al. [55] proposed a multiple-timescale transmission frame structure and associated CS-based parameter estimation algorithm for mmWave mMIMO-ISAC systems. Nevertheless, the target sensing and channel estimation in THz-mMIMO-ISAC is still in its infancy. The existing works [53], [54] typically considered the mMIMO-ISAC scenarios where the communication user and sensing target coincide as the same object, while [51], [55] investigate the mMIMO-ISAC channel estimation and target sensing at mmWave bands. In THz-mMIMO-ISAC with higher communication channel dimensions and more severe Doppler effects, along with more sensing targets that are geometrically separated from the communication user, it is still challenging to efficiently implement the communication and target sensing with the shared spectrum/hardware resources.

In this article, we investigate the problem of target sensing and channel estimation and propose an effective channel-training-aided target parameter estimation method for THz-mMIMO-ISAC systems. The main contributions of this article are summarized as follows.

1) We exploit the sparse characteristics of THz mMIMO channels and the intrinsic connection between the channel parameters and the target parameters in angular, delay, and Doppler dimensions, which enable us to integrate the target sensing functionality into the channel estimation stage. The proposed channel-training-aided

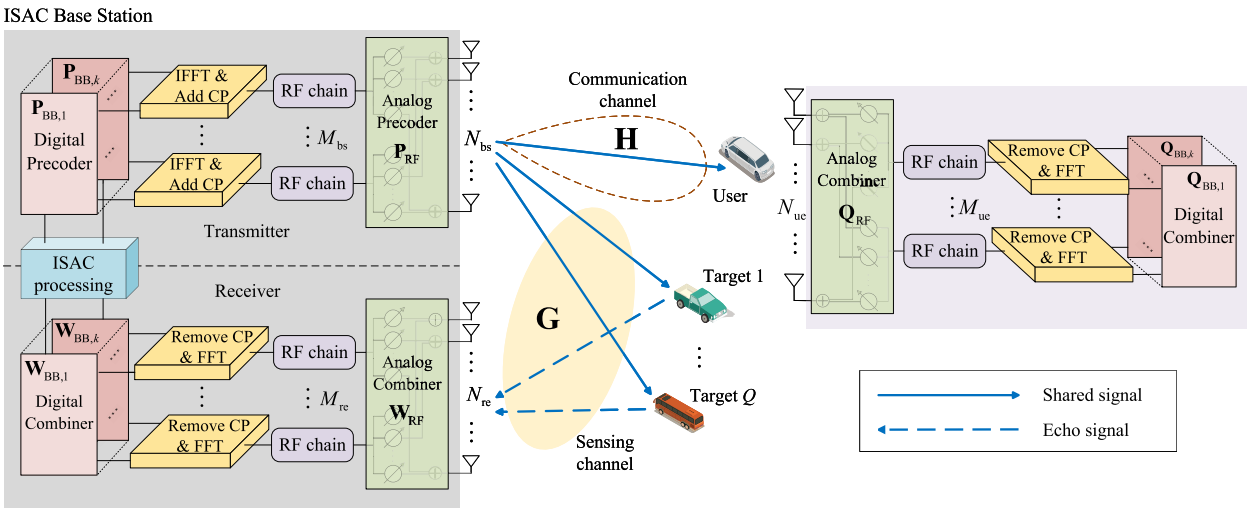

Fig. 1. Illustration of a THz-mMIMO-ISAC system, where the ISAC BS with hybrid analog and digital architectures simultaneously senses multiple targets and serves communication users.

target sensing enables to implement these two processes within a unified framework, facilitating the efficient resource sharing of THz-mMIMO-ISAC.

2) We design a shared channel training pattern accommodating the hardware constraints of hybrid transceiver architectures in THz-mMIMO-ISAC. Accordingly, the channel estimation and the target sensing can be carried out by sharing the same time–frequency resources and formulated as two structured tensor decomposition problems, which are then concurrently addressed at the user equipment (UE) and base station (BS) sides, respectively.
3) We propose a tensor-based parameter estimation algorithm to acquire the target and THz mMIMO channel parameters at the BS and UE sides, respectively. Based on the echo and received signals, the associated angles, time delays, Doppler shifts, and coefficients can be extracted from the estimated factor matrices. The proposed algorithm can overcome the low-dimensional observations brought by the hybrid architectures and the small number of training subcarriers.
4) We present the detailed derivation of Cramér–Rao bound (CRB) for the considered parameter estimation problem in THz-mMIMO-ISAC. The derived CRB can describe the best asymptotically achievable behavior of target sensing and evaluate the performance of our proposed algorithm. Simulation results demonstrate the superiority of the proposed algorithm and the estimation accuracy of target parameters is close to their corresponding CRBs.

Notations: Vectors and matrices are denoted by lowercase and uppercase boldface letters, respectively. $(\cdot)^{\mathrm{T}}$, $(\cdot)^*$, $(\cdot)^H$, and $(\cdot)^\dagger$ represent the transpose, conjugate, conjugate transpose, and Moore–Penrose pseudo-inverse operations, respectively. $\mathbf{I}_M$ is the $M \times M$ identity matrix and $j = \sqrt{-1}$ denotes an imaginary unit. $\|\cdot\|_2$ and $\|\cdot\|_F$ denote the l_2 norm and Frobenius norm, respectively. $\odot$, $\otimes$, and $\circ$ denote the Khatri–Rao product, Kronecker product, and outer product, respectively. $\mathrm{Re}\{\cdot\}$ extracts the real part of a complex number. $\mathbb{E}\{\cdot\}$ and $\mathrm{Tr}\{\cdot\}$ denote the expectation operation and trace operation, respectively. $\mathcal{CN}(0, \sigma^2)$ denotes the zero mean circularly symmetric complex Gaussian distribution with the variance of σ^2. $[\mathbf{a}]_m$ and $[\mathbf{A}]_{m,n}$ denote the mth entry and (m, n)th entry of $\mathbf{a}$ and $\mathbf{A}$, respectively. $\mathrm{diag}(\mathbf{a})$ denotes a diagonal matrix formed by $\mathbf{a}$, while $\mathrm{vec}(\mathbf{A})$ denotes the vectorization operation to a matrix $\mathbf{A}$. $\mathcal{U}[a, b]$ denotes the uniform distribution between integers a and b. $\mathbf{A}^{(K_1,1)} = [\mathbf{A}^{(1)}]_{1:K_1,:}$ denotes the submatrix that extracts the first K_1 rows of $\mathbf{A}^{(1)}$.

II. System and Channel Models of THz-mMIMO-ISAC

A. System Description

As shown in Fig. 1, we consider a THz-mMIMO-ISAC system, where the ISAC BS simultaneously senses multiple targets and serves a communication UE.[1] The BS employs the HAD architectures with N_{bs} transmit antennas and M_{bs} RF chains, while the UE is equipped with N_{ue} receive antennas and M_{ue} RF chains. To collect the echo signals reflected by the radar sensing targets, we employ an extra hardware-efficient receive array with N_{re} antennas and M_{re} RF chains at the BS, which can avoid the self-interference even without the full-duplex capability [56]. The total number of OFDM subcarriers is K with a subcarrier spacing $\Delta f = (B/K)$, where B is the system bandwidth. After the inverse fast Fourier transform (IFFT), the cyclic prefix (CP) is added to avoid the intersymbol interference caused by both the maximum channel delay spread and the time delay corresponding to the maximum detectable range. Let $\mathbf{s}_{n,k} \in \mathbb{C}^{M_{\mathrm{bs}} \times 1}$ be the ISAC symbol of the nth OFDM symbol at the kth subcarrier, the transmitted ISAC signal broadcasted by the BS can be written as

$$\mathbf{x}_{n,k} = \mathbf{P}_{\mathrm{RF}} \mathbf{P}_{\mathrm{BB},k} \mathbf{s}_{n,k} \tag{1}$$

where $\mathbf{P}_{\mathrm{RF}} \in \mathbb{C}^{N_{\mathrm{bs}} \times M_{\mathrm{bs}}}$ is the analog RF precoder and common for all subcarriers, and $\mathbf{P}_{\mathrm{BB},k} \in \mathbb{C}^{M_{\mathrm{bs}} \times M_{\mathrm{bs}}}$ denotes the digital

[1] It can be directly extended to the multiuser scenarios, since the common downlink signals are broadcasted from the BS and multiple communication UEs can estimate their downlink channels independently.

baseband precoder at the kth subcarrier. The transmitted signal satisfies $\|\mathbf{x}_{n,k}\|_2^2 = \rho$ and ρ is the transmit power. It should be noted that the integration of ISAC and THz mMIMO can share the same hardware and spectrum resources for sensing and communication functionalities, enabling improved spectral and energy efficiencies.

B. Channel Models of THz-mMIMO-ISAC

In this section, the channel models for both the communication and radar sensing in THz-mMIMO-ISAC are presented. Due to the severe propagation loss, the THz mMIMO channel can be characterized as [29], [57]

$$\mathbf{H}(t,f) = \alpha_0(t)\mathbf{a}_{\text{ue}}(\theta_0,f)\mathbf{a}_{\text{bs}}^{\text{T}}(\phi_0,f)e^{-j2\pi f\tau_0} + \frac{1}{\sqrt{PK_f}}\sum_{p=1}^{P}\alpha_p(t)\mathbf{a}_{\text{ue}}(\theta_p,f)\mathbf{a}_{\text{bs}}^{\text{T}}(\phi_p,f)e^{-j2\pi f\tau_p} \quad (2)$$

where $\alpha(t)$, τ, θ, and ϕ denote the coefficient, delay, AoA, and AoD of the channel path, respectively, the subscripts 0 and p denote the LoS path and the pth Non-LoS (NLoS) path of THz mMIMO channels, respectively, K_f is the Rician factor representing the energy ratio between the LoS and NLoS components. Due to the presence of Doppler effect, the channel coefficient can be expressed as $\alpha_p(t) = \alpha_p e^{j2\pi\nu_p t}$, where ν_p captures the Doppler shift of the pth path. $\mathbf{a}_{\text{bs}}(\phi_p,f) \in \mathbb{C}^{N_{\text{bs}}\times 1}$ and $\mathbf{a}_{\text{ue}}(\theta_p,f) \in \mathbb{C}^{N_{\text{ue}}\times 1}$ are the frequency-dependent array steering vectors, which are given by

$$\mathbf{a}_{\text{bs}}(\phi_p,f) = \left[1, e^{-j2\pi\left(1+\frac{f}{f_c}\right)\frac{d\sin\phi_p}{\lambda_c}}, \ldots, e^{-j2\pi\left(1+\frac{f}{f_c}\right)\frac{(N_{\text{bs}}-1)d\sin\phi_p}{\lambda_c}}\right]^{\text{T}} \quad (3)$$

$$\mathbf{a}_{\text{ue}}(\theta_p,f) = \left[1, e^{-j2\pi\left(1+\frac{f}{f_c}\right)\frac{d\sin\theta_p}{\lambda_c}}, \ldots, e^{-j2\pi\left(1+\frac{f}{f_c}\right)\frac{(N_{\text{ue}}-1)d\sin\theta_p}{\lambda_c}}\right]^{\text{T}} \quad (4)$$

respectively, where $\lambda_c = (c/f_c)$ denotes the carrier wavelength and f_c is the carrier frequency.

For the radar sensing, the sensing channel characterizes a round-trip process (from the BS to targets and then back to the BS) and can be modeled as [52], [55], [58]

$$\mathbf{G}(t,f) = \sum_{q=1}^{Q}\beta_q\mathbf{a}_{\text{re}}(\theta_q,f)\mathbf{a}_{\text{bs}}^{\text{T}}(\phi_q,f)e^{-j2\pi f\tau_q}e^{j2\pi\nu_q t} \quad (5)$$

where Q is the number of radar targets of interest, $\tau_q = (2R_q/c)$ and $\nu_q = f_c(2V_q/c)$ represent the round-trip time delay and the Doppler shift, respectively, R_q and V_q are the distance and the radial velocity of the qth target, β_q is the complex-valued reflection coefficient accounting for the radar cross section (RCS) of the qth target, ϕ_q and θ_q denote the AoD and AoA of the qth target, respectively, $\mathbf{a}_{\text{re}}(\theta_q,f) \in \mathbb{C}^{N_{\text{re}}\times 1}$ is the receive array steering vector given by

$$\mathbf{a}_{\text{re},f}(\theta_q) = \left[1, e^{-j2\pi\left(1+\frac{f}{f_c}\right)\frac{d\sin\theta_q}{\lambda_c}}, \ldots, e^{-j2\pi\left(1+\frac{f}{f_c}\right)\frac{(N_{\text{re}}-1)d\sin\theta_q}{\lambda_c}}\right]^{\text{T}}. \quad (6)$$

III. Training Pattern and Problem Formulation

In this section, we present the proposed training pattern design for simultaneous target sensing and channel training. Then, we illustrate how to leverage the proposed training pattern to facilitate the tensor-based problem formulation in THz-mMIMO-ISAC.

A. Training Pattern

Before presenting the training pattern, we first present the received signal model for sensing and communication, respectively. Given the transmitted ISAC signal in (1), the radar echo signal at the BS side can be given by

$$\bar{\mathbf{y}}_{n,k}^{\text{echo}} = \mathbf{W}_{\text{BB},k}^H\mathbf{W}_{\text{RF}}^H\mathbf{G}_{n,k}\mathbf{P}_{\text{RF}}\mathbf{P}_{\text{BB},k}\mathbf{s}_{n,k} + \mathbf{W}_{\text{BB},k}^H\mathbf{W}_{\text{RF}}^H\bar{\mathbf{n}}_{n,k}^{\text{echo}} \quad (7)$$

where $\mathbf{W}_{\text{RF}} \in \mathbb{C}^{N_{\text{re}}\times M_{\text{re}}}$ and $\mathbf{W}_{\text{BB}} \in \mathbb{C}^{M_{\text{re}}\times M_{\text{re}}}$ are the analog and digital combiners of the BS receive array, respectively, $\bar{\mathbf{n}}_{n,k}^{\text{echo}} \sim \mathcal{CN}(\mathbf{0}, \sigma_{\text{echo}}^2\mathbf{I}_{N_{\text{re}}})$ is the additive Gaussian noise vector, $\mathbf{G}_{n,k} = \mathbf{G}(t,f)|_{t=nT_{\text{sym}},f=k\Delta f}$ represents the sensing channel matrix at the kth subcarrier of the nth OFDM symbol and is given by

$$\mathbf{G}_{n,k} = \sum_{q=1}^{Q}\beta_q e^{-j2\pi\tau_q k\Delta f}\mathbf{a}_{\text{re},k}(\theta_q)\mathbf{a}_{\text{bs},k}^{\text{T}}(\phi_q)e^{j2\pi n\nu_q T_{\text{sym}}} \quad (8)$$

where $\mathbf{a}_{\text{re},k}(\theta_q) = \mathbf{a}_{\text{re}}(\theta_q,f)|_{f=k\Delta f}$, $\mathbf{a}_{\text{bs},k}(\phi_q) = \mathbf{a}_{\text{bs}}(\phi_q,f)|_{f=k\Delta f}$, $T_{\text{sym}} = 1/\Delta f + T_{\text{cp}}$ is the OFDM symbol duration, and T_{cp} denotes the CP duration.

Meanwhile, the received signals at the UE side can be expressed as

$$\bar{\mathbf{r}}_{n,k}^{\text{com}} = \mathbf{Q}_{\text{BB},k}^H\mathbf{Q}_{\text{RF}}^H\mathbf{H}_{n,k}\mathbf{P}_{\text{RF}}\mathbf{P}_{\text{BB},k}\mathbf{s}_{n,k} + \mathbf{Q}_{\text{BB},k}^H\mathbf{Q}_{\text{RF}}^H\bar{\mathbf{n}}_{n,k}^{\text{com}} \quad (9)$$

where $\mathbf{Q}_{\text{RF}} \in \mathbb{C}^{N_{\text{ue}}\times M_{\text{ue}}}$ and $\mathbf{Q}_{\text{BB}} \in \mathbb{C}^{M_{\text{ue}}\times M_{\text{ue}}}$ are the analog and digital combiners at the UE side; $\mathbf{H}_{n,k} = \mathbf{H}(t,f)|_{t=nT_{\text{sym}},f=k\Delta f}$ represents communication channel matrix; $\bar{\mathbf{n}}_{n,k}^{\text{com}} \sim \mathcal{CN}(\mathbf{0}, \sigma_{\text{com}}^2\mathbf{I}_{N_{\text{ue}}})$ is the additive Gaussian noise vector.

Our goal is to exploit the transmitted ISAC signaling for both the estimation of the THz communication channel $\mathbf{H}_{n,k}$ and the target parameters contained in $\mathbf{G}_{n,k}$. Due to the presence of HAD architectures, however, either for the sensing channel $\mathbf{G}_{n,k}$ or the communication channel $\mathbf{H}_{n,k}$, the dimension of the observations $\bar{\mathbf{y}}_{n,k}^{\text{echo}}$ or $\bar{\mathbf{r}}_{n,k}^{\text{echo}}$ after hybrid combining is lower than the dimension of channel matrices. Moreover, due to the time-varying characteristics induced by Doppler effects, of the high dimensional matrix $\mathbf{G}_{n,k}$, the unknown channel coefficients of the high-dimensional channel matrix will accordingly increase as we accumulate more observations over time. The aforementioned issues make the acquisition of the channel and target parameters quite challenging within the limited coherent time.

To this end, we propose a shared training pattern that meets the practical hardware constraints imposed by the hybrid architectures and facilitates both the channel training and the target sensing. Specifically, the shared training pattern

is constructed to satisfy $\mathbf{s}_{n,k} = \mathbf{U}_{\mathbf{P},k}\mathbf{t}_n s_k$, where $\mathbf{U}_{\mathbf{P},k} \in \mathbb{C}^{M_{\text{bs}} \times M_{\text{bs}}}$ is a unitary matrix enforcing $\mathbf{P}_{\text{BB},k}\mathbf{U}_{\mathbf{P},k}$ is frequency-flat, $\mathbf{t}_n \in \mathbb{C}^{M_{\text{bs}} \times 1}$ is the training precoder and $s_k \in \mathbb{C}$ is the training symbol satisfying $|s_k|^2 = 1$. In this way, the transmit signal $\mathbf{x}_{n,k} \triangleq \mathbf{P}_{\text{RF}}\mathbf{P}_{\text{BB},k}\mathbf{s}_{n,k}$ can be expressed as $\mathbf{x}_{n,k} = \mathbf{p}_n s_k$, where $\mathbf{p}_n \triangleq \mathbf{P}_{\text{RF}}\mathbf{P}_{\text{BB},k}\mathbf{U}_{\mathbf{P},k}\mathbf{t}_n$. Note that $\mathbf{p}_n$ varies for different OFDM symbols while s_k remains unchanged during the training stage. At the receiver side, we employ the frequency-flat combiners during the training phase, i.e., $\mathbf{W} = \mathbf{W}_{\text{RF}}\mathbf{W}_{\text{BB},k} = \mathbf{W}_{\text{RF}}(\mathbf{W}_{\text{RF}}^H\mathbf{W}_{\text{RF}})^{-(1/2)}$, to keep the low hardware and computational complexity.

As shown in the next section, the proposed channel training pattern will subsequently assist to formulate the received signals as the tensor format, which can capture the intrinsic multidimensional structure of the high-dimensional and time-varying communication/sensing channels from the perspective of space, time, and frequency domains.

B. Problem Formulation

In this section, we elaborate how to exploit the proposed training pattern to facilitate the tensor-based problem formulation for both target and channel parameters estimation. Specifically, after removing the training symbol at the receiver, the echo signals (7) can be written as (10), shown at the bottom of the page, where $\mathbf{n}_{n,k} = s_k^* \mathbf{W}^H \bar{\mathbf{n}}_{n,k}^{\text{echo}}$ is the corresponding noise vector. Concatenating the echo signals of the N_{tr} training OFDM symbols yields

$$\mathbf{Y}_k = \sum_{q=1}^{Q} \beta_q e^{-j2\pi\tau_q k\Delta f} \mathbf{W}^H \mathbf{a}_{\text{re},k}(\theta_q)\mathbf{a}_{\text{bs},k}^{\text{T}}(\phi_q)\mathbf{P}\boldsymbol{\Gamma}(\nu_q) + \mathbf{N}_k \tag{11}$$

where $\mathbf{Y}_k = [\mathbf{y}_{1,k}, \mathbf{y}_{2,k}, \ldots, \mathbf{y}_{N_{\text{tr}},k}] \in \mathbb{C}^{M_{\text{re}} \times N_{\text{tr}}}$ contains the overall echo signals at the kth subcarrier; $\boldsymbol{\Gamma}(\nu_q) \in \mathbb{C}^{N_{\text{tr}} \times N_{\text{tr}}}$ is a diagonal matrix with the nth diagonal entry being $e^{j2\pi n\nu_q T_{\text{sym}}}$; $\mathbf{P} = [\mathbf{p}_1, \ldots, \mathbf{p}_{N_{\text{tr}}}] \in \mathbb{C}^{N_{\text{bs}} \times N_{\text{tr}}}$ is the training precoder matrix and $\mathbf{N}_k = [\mathbf{n}_1, \ldots, \mathbf{n}_{N_{\text{tr}}}] \in \mathbb{C}^{M_{\text{re}} \times N_{\text{tr}}}$ denotes the noise matrix. Due to the frequency-dependent $\mathbf{a}_{\text{re},k}$ and $\mathbf{a}_{\text{bs},k}$ in THz-mMIMO-ISAC, the echo signals in (11) cannot be directly decomposed into independent multiple dimensions, thus not admit to the tensor model. To address this issue, we leverage a small portion of the subcarriers $|\mathcal{K}_{\text{tr}}| = K_{\text{tr}}$ as the training subcarriers, such that $\mathbf{a}_{\text{re}} \approx \mathbf{a}_{\text{re},k}$ and $\mathbf{a}_{\text{bs}} \approx \mathbf{a}_{\text{bs},k}$ for $k \in \mathcal{K}_{\text{tr}}$. In this case, the steering vectors becomes almost frequency-independent and the beam squint effect can be mitigated. Accordingly, the (m, n)th entry of $\mathbf{Y}_k$ can be given by

$$[\mathbf{Y}_k]_{m,n} = \sum_{q=1}^{Q} \beta_q e^{-j2\pi\tau_q k\Delta f} \left[\mathbf{b}_{\text{re}}(\theta_q)\right]_m \left[\mathbf{b}_{\text{bs}}(\phi_q, \nu_q)\right]_n + [\mathbf{N}_k]_{m,n} \tag{12}$$

where $\mathbf{b}_{\text{re}}(\theta_q) = \mathbf{W}^H\mathbf{a}_{\text{re}}(\theta_q)$ and $\mathbf{b}_{\text{bs}}(\phi_q, \nu_q) = \boldsymbol{\Gamma}(\nu_q)\mathbf{P}^{\text{T}}\mathbf{a}_{\text{bs}}(\phi_q)$ are the equivalent steering vectors. From (12) and Appendix A, we can observe that the echo signals conform to a third-order tensor $\boldsymbol{\mathcal{Y}} \in \mathbb{C}^{M_{\text{re}} \times N_{\text{tr}} \times K_{\text{tr}}}$ with its (m, n, k)th element being $[\mathbf{Y}_k]_{m,n}$ [59], yielding

$$\begin{aligned}\boldsymbol{\mathcal{Y}} &= \sum_{q=1}^{Q} \beta_q \mathbf{b}_{\text{re}}(\theta_q) \circ \mathbf{b}_{\text{bs}}(\phi_q, \nu_q) \circ \mathbf{a}_{\text{td}}(\tau_q) + \boldsymbol{\mathcal{N}} \\ &= [\![\mathbf{C}^{(1)}, \mathbf{C}^{(2)}, \mathbf{C}^{(3)}]\!] + \boldsymbol{\mathcal{N}}\end{aligned} \tag{13}$$

where $\boldsymbol{\mathcal{N}} \in \mathbb{C}^{M_{\text{re}} \times N_{\text{tr}} \times K_{\text{tr}}}$ is the noise tensor, and the three factor matrices are expressed as

$$\mathbf{C}^{(1)} \triangleq \left[\beta_1 \mathbf{b}_{\text{re}}(\theta_1), \ldots, \beta_Q \mathbf{b}_{\text{re}}(\theta_Q)\right] \in \mathbb{C}^{M_{\text{re}} \times Q} \tag{14}$$

$$\mathbf{C}^{(2)} \triangleq \left[\mathbf{b}_{\text{bs}}(\phi_1, \nu_1), \ldots, \mathbf{b}_{\text{bs}}(\phi_Q, \nu_Q)\right] \in \mathbb{C}^{N_{\text{tr}} \times Q} \tag{15}$$

$$\mathbf{C}^{(3)} \triangleq \left[\mathbf{a}_{\text{td}}(\tau_1), \ldots, \mathbf{a}_{\text{td}}(\tau_Q)\right] \in \mathbb{C}^{K_{\text{tr}} \times Q} \tag{16}$$

where $\mathbf{a}_{\text{td}}(\tau_q)$ is defined as

$$\mathbf{a}_{\text{td}}(\tau_q) = \left[e^{-j2\pi\tau_q\Delta f}, \ldots, e^{-j2\pi\tau_q K_{\text{tr}}\Delta f}\right]^{\text{T}}. \tag{17}$$

Note that our goal is to estimate the unknown target parameters $\{\theta_q, \phi_q, \nu_q, \tau_q, \beta_q\}_{q=1}^Q$ and the target sensing problem can be formulated as

$$\underset{\substack{\{\theta_q,\phi_q,\nu_q,\\ \tau_q,\beta_q\}_{q=1}^Q}}{\text{minimize}} \left\|\boldsymbol{\mathcal{Y}} - \sum_{q=1}^{Q} \beta_q \mathbf{b}_{\text{re}}(\theta_q) \circ \mathbf{b}_{\text{bs}}(\phi_q, \nu_q) \circ \mathbf{a}_{\text{td}}(\tau_q)\right\|_F^2. \tag{18}$$

Meanwhile, the received training signals at the UE side are employed for channel estimation. Thanks to the proposed shared training pattern, the channel estimation problem can be represented as a third-order tensor via the similar modeling method as the echo signals given by (11)–(16). Consequently, the channel estimation problem can be similarly formulated as

$$\underset{\substack{\{\theta_p,\phi_p,\nu_p,\\ \tau_p,\alpha_p\}_{p=0}^P}}{\text{minimize}} \left\|\boldsymbol{\mathcal{R}} - \sum_{p=0}^{P} \alpha_p \mathbf{b}_{\text{ue}}(\theta_p) \circ \mathbf{b}_{\text{bs}}(\phi_p, \nu_p) \circ \mathbf{a}_{\text{td}}(\tau_p)\right\|_F^2 \tag{19}$$

where $\boldsymbol{\mathcal{R}} \in \mathbb{C}^{M_{\text{ue}} \times N_{\text{tr}} \times K_{\text{tr}}}$ is the observation tensor at the UE side, $\mathbf{b}_{\text{ue}}(\theta_p) = \mathbf{Q}^H\mathbf{a}_{\text{ue}}(\theta_p)$ and $\mathbf{Q} \in \mathbb{C}^{N_{\text{ue}} \times M_{\text{ue}}}$ is the combining matrix at the UE side.

From (18) and (19), we can observe that both the target sensing and channel estimation problems exhibit the mathematical expression. Nevertheless, the unknown parameters $\{\theta_q, \phi_q, \tau_q, \beta_q, \nu_q\}_{q=1}^Q$ or $\{\theta_p, \phi_p, \tau_p, \beta_p, \nu_p\}_{p=0}^P$ are nonlinearly coupled together and it is challenging to perform the joint optimization directly.

IV. Proposed Target Parameter and Channel Estimation Algorithm

In this section, we will propose a tensor-based target parameter and channel estimation algorithm for THz-mMIMO-ISAC. We first illustrate how to obtain the estimation of factor matrices that incorporate the unknown target parameters. Then, we show how to extract the target parameters based on

$$\mathbf{y}_{n,k} = s_k^* \bar{\mathbf{y}}_{n,k}^{\text{echo}} = \sum_{q=1}^{Q} \beta_q e^{-j2\pi\tau_q k\Delta f} \mathbf{W}^H \mathbf{a}_{\text{re},k}(\theta_q)\mathbf{a}_{\text{bs},k}^{\text{T}}(\phi_q)\mathbf{p}_n \cdot e^{j2\pi n\nu_q T_{\text{sym}}} + \mathbf{n}_{n,k} \tag{10}$$

the estimated factor matrices. Finally, we will explain how to leverage the proposed parameter estimation algorithm for estimating the THz mMIMO channels.

A. Estimation of Factor Matrices

Since the unknown parameters are incorporated in the factor matrices, one effective strategy is to first estimate the factor matrices from the tensor $\mathcal{Y}$ in (13). One of the most well-known algorithms for factor matrices estimation is the alternating least-squares (ALSs)-based algorithm [42], [46], [60]. This algorithm, however, generally does not utilize any structured information of factor matrices. For the considered problem in (18), we notice that the factor matrix $\mathbf{C}^{(3)}$ exhibits an inherent Vandermonde structure. With this structural information at hand, we can apply the spatial smoothing technique for the factor matrices estimation and enhance the parameter estimation performance [44], [61]. To be specific, taking the matrix unfolding of $\mathcal{Y}$ along its first dimension and the transpose operation, we have

$$\mathbf{Y}_{(1)}^{\mathrm{T}} = \mathbf{C}^{(3,2)}\mathbf{C}^{(1)\mathrm{T}} + \mathbf{N}_{(1)}^{\mathrm{T}} \tag{20}$$

where $\mathbf{C}^{(3,2)} = \mathbf{C}^{(3)} \odot \mathbf{C}^{(2)}$ is defined, and $\mathbf{N}_{(1)} \in \mathbb{C}^{M_{\mathrm{re}} \times K_{\mathrm{tr}} N_{\mathrm{tr}}}$ is the corresponding noise matrix. Denote the generators of the Vandermonde-structured $\mathbf{C}^{(3)}$ as $\{z_{\tau,q} = e^{-j2\pi\tau_q \Delta f}\}_{q=1}^{Q}$ and generate a cyclic selection matrix $\mathbf{J}_{l_3} = [\mathbf{0}_{K_3 \times l_3 - 1} \ \mathbf{I}_{K_3} \ \mathbf{0}_{K_3 \times L_3 - l_3}] \otimes \mathbf{I}_{N_{\mathrm{tr}}} \in \mathbb{C}^{K_3 N_{\mathrm{tr}} \times K_{\mathrm{tr}} N_{\mathrm{tr}}}$, where $l_3 \in \{1, 2, \ldots, L_3\}$, $L_3 = K_{\mathrm{tr}} + 1 - K_3$, $K_3 \in \{1, 2, \ldots, K_{\mathrm{tr}}\}$. We can construct the augmented received signal as follows:

$$\begin{aligned}\mathbf{Y}_S &= \left[\mathbf{J}_1 \mathbf{Y}_{(1)}^{\mathrm{T}} \ \cdots \ \mathbf{J}_{L_3} \mathbf{Y}_{(1)}^{\mathrm{T}}\right] \\ &= \left[\mathbf{J}_1 \mathbf{C}^{(3,2)} \ \cdots \ \mathbf{J}_{L_3} \mathbf{C}^{(3,2)}\right] \left(\mathbf{I}_{L_3} \otimes \mathbf{C}^{(1)}\right)^{\mathrm{T}} + \mathbf{N}_S \\ &= \left(\mathbf{C}^{(K_3,3)} \odot \mathbf{C}^{(2)}\right) \mathbf{\Lambda}^{-1} \left(\mathbf{C}^{(L_3,3)} \odot \mathbf{C}^{(1)}\right)^{\mathrm{T}} + \mathbf{N}_S \end{aligned} \tag{21}$$

where the equalities exploit the generator property $z_{\tau,q}^{K_{\mathrm{tr}}} = z_{\tau,q}^{K_3 + L_3 - 1}$, $\mathbf{\Lambda} \in \mathbb{C}^{Q \times Q}$ is a diagonal matrix whose qth element being $z_{\tau,q}$, $\mathbf{N}_S \in \mathbb{C}^{K_3 N_{\mathrm{tr}} \times L_3 M_{\mathrm{re}}}$ is the corresponding noise matrix. Given the augmented received signal $\mathbf{Y}_S$, we can obtain the estimation of factor matrices based on Theorem 1.

Theorem 1: Denote the singular value decomposition $\mathbf{Y}_S = \mathbf{U}_s \mathbf{\Sigma}_s \mathbf{V}_s^H + \mathbf{U}_n \mathbf{\Sigma}_n \mathbf{V}_n^H$, where $\mathbf{U}_s \in \mathbb{C}^{K_3 N_{\mathrm{tr}} \times Q}$ and $\mathbf{V}_s \in \mathbb{C}^{L_3 M_{\mathrm{re}} \times Q}$ are the signal subspaces spanned by the Q principal singular vectors, respectively. Then, the estimation of factor matrices of $\mathcal{Y}$ can be obtained by

$$\hat{\mathbf{C}}^{(1)} = \left(\left(\hat{\mathbf{C}}^{(3)} \odot \hat{\mathbf{C}}^{(2)}\right)^{\dagger} \mathbf{Y}_{(1)}^{\mathrm{T}}\right)^{\mathrm{T}} \tag{22}$$

$$\hat{\mathbf{C}}^{(2)} = \left[\hat{\mathbf{c}}_1^{(2)}, \ldots, \hat{\mathbf{c}}_Q^{(2)}\right] \tag{23}$$

$$\hat{\mathbf{C}}^{(3)} = \left[\hat{\mathbf{c}}_1^{(3)}, \ldots, \hat{\mathbf{c}}_Q^{(3)}\right] \tag{24}$$

where the qth column of $\hat{\mathbf{C}}^{(2)}$ and $\hat{\mathbf{C}}^{(3)}$ can be, respectively, given by

$$\hat{\mathbf{c}}_q^{(2)} = \left(\frac{\hat{\mathbf{c}}_q^{(K_3,3)H}}{\left\|\hat{\mathbf{c}}_q^{(K_3,3)}\right\|_2^2} \otimes \mathbf{I}_{N_{\mathrm{tr}}}\right) \mathbf{U}_s \mathbf{m}_q \tag{25}$$

$$\hat{\mathbf{c}}_q^{(3)} = \left[\hat{z}_{\tau,q}, \hat{z}_{\tau,q}^2, \ldots, \hat{z}_{\tau,q}^{K_{\mathrm{tr}}}\right]^{\mathrm{T}} \tag{26}$$

where $\hat{z}_{\tau,q}$ and $\mathbf{m}_q$ are the qth normalized eigenvalue and eigenvector of the matrix $\mathbf{U}_1^{\dagger}\mathbf{U}_2$, respectively, and $\mathbf{U}_1 = [\mathbf{U}_s]_{1:(K_3-1)N_{\mathrm{tr}},:}$, $\mathbf{U}_2 = [\mathbf{U}_s]_{N_{\mathrm{tr}}+1:K_3 N_{\mathrm{tr}},:}$, and $\hat{\mathbf{c}}_q^{(K_3,3)} = [\hat{\mathbf{c}}_q^{(3)}]_{1:K_3}$.

Proof: See Appendix B. ■

Theorem 1 provides a means of estimating the factor matrices that incorporate the whole information about unknown parameters θ_q, ϕ_q, τ_q, ν_q, and β_q. Note that the estimated factor matrices from Theorem 1 are not exactly the original one defined in (14)–(16), but suffer from column permutation and scaling ambiguity. Specifically, the estimated and true factor matrices satisfy the relationship as follows:

$$\hat{\mathbf{C}}^{(i)} \triangleq \mathbf{C}^{(i)} \mathbf{\Pi} \mathbf{\Delta}^{(i)} + \mathbf{E}^{(i)} \tag{27}$$

where $\mathbf{\Pi} \in \mathbb{C}^{Q \times Q}$ denotes a permutation matrix, and $\mathbf{\Delta}^{(i)}$ and $\mathbf{E}^{(i)}$ represent the unknown diagonal matrix and the errors of tensor factorization, respectively, $i = 1, 2, 3$. Fortunately, the column permutation and scaling ambiguity do not destroy the pairing relation between the factor matrices $\hat{\mathbf{C}}^{(i)}$ and $\mathbf{C}^{(i)}$, allowing the unknown parameters to be extracted from the corresponding factor matrix. In the following, we will show how to leverage the estimated factor matrices for parameters estimation.

B. Estimation of Unknown Parameters

In this section, we turn to the estimation of unknown parameters θ_q, ϕ_q, τ_q, β_q, and ν_q using the estimated factor $\{\hat{\mathbf{C}}^{(1)}, \hat{\mathbf{C}}^{(2)}, \hat{\mathbf{C}}^{(3)}\}$.

By observing the relationship of factor matrices in (27), we find that each column of $\hat{\mathbf{C}}^{(1)}$ is paired with one AoA. Accordingly, we can separately extract the AoA θ_q via the correlation-based method with respect to each column of $\hat{\mathbf{C}}^{(1)}$ [42], i.e.,

$$\hat{\theta}_q = \arg\max_{\theta_q} \frac{\left|\left(\hat{\mathbf{c}}_q^{(1)}\right)^H \mathbf{b}_{\mathrm{re}}(\theta_q)\right|^2}{\left\|\hat{\mathbf{c}}_q^{(1)}\right\|_2^2 \left\|\mathbf{b}_{\mathrm{re}}(\theta_q)\right\|_2^2}, \quad q = 1, \ldots, Q \tag{28}$$

where $\hat{\mathbf{c}}_q^{(1)}$ is the qth column of the estimated factor matrix $\hat{\mathbf{C}}^{(1)}$. Similarly, since the parameter of time delays is associated with the factor matrix $\hat{\mathbf{C}}^{(3)}$, then the time delay $\{\hat{\tau}_q\}$ of the qth target can be estimated as follows:

$$\hat{\tau}_q = \arg\max_{\tau_q} \frac{\left|\left(\hat{\mathbf{c}}_q^{(3)}\right)^H \mathbf{a}_{\mathrm{td}}(\tau_q)\right|^2}{\left\|\hat{\mathbf{c}}_q^{(3)}\right\|_2^2 \left\|\mathbf{a}_{\mathrm{td}}(\tau_q)\right\|_2^2}, \quad q = 1, \ldots, Q. \tag{29}$$

Now, we turn to the estimation of Doppler shifts and AoDs via the estimated factor matrix $\hat{\mathbf{C}}^{(2)}$. For the qth column of $\hat{\mathbf{C}}^{(2)}$, we have $\hat{\mathbf{c}}_q^{(2)} = \delta_q \mathbf{\Gamma}(\nu_q) \mathbf{P}^{\mathrm{T}} \mathbf{a}_{\mathrm{bs}}(\phi_q) + \mathbf{e}_q$, where δ_q is the qth diagonal element of $\mathbf{\Delta}^{(2)}$ and $\mathbf{e}_q$ is the qth column of $\mathbf{E}^{(2)}$. Our goal is to estimate the AoD ϕ_q and the Doppler shift ν_q from $\hat{\mathbf{c}}_q^{(2)}$, which can be formulated as

$$\{\hat{\nu}_q, \hat{\phi}_q\} = \arg\min_{\nu_q, \phi_q} \left\|\hat{\mathbf{c}}_q^{(2)} - \delta_q \mathbf{\Gamma}(\nu_q) \mathbf{P}^{\mathrm{T}} \mathbf{a}_{\mathrm{bs}}(\phi_q)\right\|_2^2. \tag{30}$$

Different from (28) and (29) only dealing with one parameter, we need leverage (30) to simultaneously handle two coupled parameters, i.e., ν_q and ϕ_q. In addition, since the unknown Doppler shift ν_q introduces extra phase offsets, which will degrade the AoD estimation performance if simply

ignoring the phase offsets [46]. The aforementioned issues pose challenges for the accurate estimation of AoDs and Doppler shifts. To this end, we propose to iteratively refine the estimate of AoD $\hat{\phi}_q$ and the Doppler shift $\hat{\nu}_q$ until the iterative process converges to a stationary point. To be specific, let $\hat{\nu}_q^{[i-1]}$ be the Doppler shift estimate at the $(i-1)$th iteration, then the estimation of the AoD can be given by

$$\begin{aligned}\{\hat{\phi}_q^{[i]}\} &= \arg\min_{\phi_q} \left\| \hat{\mathbf{c}}_q^{(2)} - \delta_q \mathbf{\Gamma}\left(\hat{\nu}_q^{[i-1]}\right)\mathbf{P}^{\mathrm{T}}\mathbf{a}_{\mathrm{bs}}(\phi_q)\right\|_2^2 \\ &= \arg\min_{\phi_q} \left\| \hat{\mathbf{d}}_q^{[i-1]} - \delta_q \mathbf{P}^{\mathrm{T}}\mathbf{a}_{\mathrm{bs}}(\phi_q)\right\|_2^2 \end{aligned} \tag{31}$$

where the second equality holds by defining $\hat{\mathbf{d}}_q^{[i-1]} = \mathbf{\Gamma}^{-1}(\hat{\nu}_q^{[i-1]})\hat{\mathbf{c}}_q^{(2)}$. Then, when we have estimated AoD $\hat{\phi}_q^{[i]}$ at hand, the problem (30) degenerates to

$$\begin{aligned}\{\hat{\nu}_q^{[i]}\} &= \arg\min_{\nu_q} \left\| \hat{\mathbf{c}}_q^{(2)} - \delta_q \mathbf{\Gamma}(\nu_q)\mathbf{P}^{\mathrm{T}}\mathbf{a}_{\mathrm{bs}}\left(\hat{\phi}_q^{[i]}\right)\right\|_2^2 \\ &= \arg\min_{\nu_q} \left\| \hat{\mathbf{c}}_q^{(2)} - \delta_q \mathbf{\Psi}^{\mathrm{T}}\mathbf{a}_{\mathrm{do}}(\nu_q)\right\|_2^2 \end{aligned} \tag{32}$$

where the second equality comes from introducing a matrix $\mathbf{\Psi}$ with its diagonal elements being $\mathbf{P}^{\mathrm{T}}\mathbf{a}_{\mathrm{bs}}(\hat{\phi}_q^{[i]})$, and $\mathbf{a}_{\mathrm{do}}(\nu_q)$ comes from the diagonal elements of $\mathbf{\Gamma}(\nu_q)$ and is given by

$$\mathbf{a}_{\mathrm{do}}(\nu_q) = \left[e^{j2\pi\nu_q T_{\mathrm{sym}}}, e^{j4\pi\nu_q T_{\mathrm{sym}}}, \ldots, e^{j2\pi N_{\mathrm{tr}}\nu_q T_{\mathrm{sym}}}\right]^{\mathrm{T}}. \tag{33}$$

From (31) and (32), we can find that the joint estimation problem (30) is separated into two individual problems for AoD and Doppler shift, respectively. These two problems are alternately solved and will gradually decrease the objective function value of problem (30) as the number of iterations i increases, thus converging to a stationary solution of the problem (30). Due to the similar mathematical forms, the estimate for $\hat{\phi}_q^{[i]}$ and $\hat{\nu}_q^{[i]}$ at the ith iteration can be, respectively, given by

$$\hat{\phi}_q^{[i]} = \arg\max_{\phi_q} \frac{\left|\left(\hat{\mathbf{d}}_q^{[i-1]}\right)^H \mathbf{P}^{\mathrm{T}}\mathbf{a}_{\mathrm{bs}}(\phi_q)\right|^2}{\left\|\hat{\mathbf{d}}_q^{[i-1]}\right\|_2^2 \left\|\mathbf{P}^{\mathrm{T}}\mathbf{a}_{\mathrm{bs}}(\phi_q)\right\|_2^2} \tag{34}$$

$$\hat{\nu}_q^{[i]} = \arg\max_{\nu_q} \frac{\left|\left(\hat{\mathbf{c}}_q^{(2)}\right)^H \mathbf{\Psi}^{\mathrm{T}}\mathbf{a}_{\mathrm{do}}(\nu_q)\right|^2}{\left\|\hat{\mathbf{c}}_q^{(2)}\right\|_2^2 \left\|\mathbf{\Psi}^{\mathrm{T}}\mathbf{a}_{\mathrm{do}}(\nu_q)\right\|_2^2}. \tag{35}$$

When the iteration converges to a stationary point, we can obtain the final estimate of AoD and Doppler shift as $\hat{\phi}_q$ and $\hat{\nu}_q$, respectively. By performing the estimation for each column of factor matrices $\{\hat{\mathbf{C}}^{(1)}, \hat{\mathbf{C}}^{(2)}, \hat{\mathbf{C}}^{(3)}\}$, we can obtain $\{\hat{\nu}_q\}_{q=1}^Q$, $\{\hat{\phi}_q\}_{q=1}^Q$, $\{\hat{\theta}_q\}_{q=1}^Q$, and $\{\hat{\tau}_q\}_{q=1}^Q$. Next, we will show how to estimate the reflection coefficients. Based on the tensor model of echo signals in (20), by taking its vectorization operation, we can obtain

$$\mathrm{vec}\left(\mathbf{Y}_{(1)}^{\mathrm{T}}\right) = \mathbf{B}^{(1)} \odot \left(\mathbf{C}^{(3)} \odot \mathbf{C}^{(2)}\right)\boldsymbol{\beta} + \mathrm{vec}\left(\mathbf{N}_{(1)}^{\mathrm{T}}\right) \tag{36}$$

where we introduce $\mathbf{B}^{(1)} = [\mathbf{b}_{\mathrm{re}}(\theta_1), \ldots, \mathbf{b}_{\mathrm{re}}(\theta_Q)]$ and $\boldsymbol{\beta} = [\beta_1, \ldots, \beta_Q]^{\mathrm{T}}$. From (36), the reflection coefficients can be estimated via the least-squares criterion, yielding

$$\hat{\boldsymbol{\beta}} = \left(\hat{\mathbf{C}}^{(3)} \odot \left(\hat{\mathbf{C}}^{(2)} \odot \hat{\mathbf{B}}^{(1)}\right)\right)^{\dagger} \mathrm{vec}\left(\mathbf{Y}_{(3)}^{\mathrm{T}}\right) \tag{37}$$

Algorithm 1 Proposed Target Parameter Estimation Algorithm

Input: $\mathcal{Y}$, $\mathbf{P}$, $\mathbf{W}$, initial Doppler shift $\nu_q^{[0]} = 0$, the number of iterations I_{iter}.

1: Compute the factor matrices $\mathbf{C}^{(3)}$, $\mathbf{C}^{(2)}$, and $\mathbf{C}^{(1)}$ via Theorem 1;
2: **for** each $q \in [1, \ldots, Q]$ **do**
3: Estimate $\hat{\theta}_q$ and $\hat{\tau}_q$ via (28) and (29), respectively;
4: **for** $i = 1, \ldots, I_{\mathrm{iter}}$ **do**
5: Estimate $\hat{\phi}_q^{[i]}$ and $\hat{\nu}_q^{[i]}$ via (31) and (32), respectively;
6: **end for**
7: Return $\hat{\phi}_q = \phi_q^{[I_{\mathrm{iter}}]}$ and $\hat{\nu}_q = \nu_q^{[I_{\mathrm{iter}}]}$;
8: **end for**
9: Estimate $\hat{\beta}_q$ via (37);

Output: Return $\{\hat{\theta}_q, \hat{\tau}_q, \hat{\phi}_q, \hat{\nu}_q, \hat{\beta}_q\}_{q=1}^Q$.

where $\hat{\mathbf{C}}^{(3)}$ is constructed based on $\{\hat{\tau}_q\}_{q=1}^Q$, $\hat{\mathbf{B}}^{(1)}$ is constructed based on $\{\hat{\theta}_q\}_{q=1}^Q$, and $\hat{\mathbf{C}}^{(2)}$ is constructed based on $\{\hat{\nu}_q\}_{q=1}^Q$ and $\{\hat{\phi}_q\}_{q=1}^Q$. We summarize the proposed target parameter estimation algorithm in Algorithm 1. The superiority of the proposed Algorithm 1 includes two aspects. On the one hand, the inherent Vandermonde structure of $\mathbf{C}^{(3)}$ is exploited for the estimation of factor matrices. On the other hand, the proposed algorithm can simultaneously estimate the delay, Doppler, and angular parameters of the target or channel via the same signals, facilitating the channel-training-aided target sensing in THz-mMIMO-ISAC systems.

C. Communication Channel Estimation

In this section, we present how to perform the channel estimation at the UE side. Due to the limited scattering and reflection characteristics of THz mMIMO channels, instead of explicitly estimating the high-dimensional channel, we turn to estimate the finite physical channel parameters, i.e., $\{\theta_p, \phi_p, \tau_p, \beta_p, \nu_p\}_{p=0}^P$, thereby making it possible to reconstruct THz mMIMO channels using the reduced training overhead. Thanks to the proposed training pattern, we can model the channel estimation problem as (19), which exhibits similar mathematical formulation as target parameter estimation problem in (18). The difference lies on different physical meanings, such as τ_p and ν_p denote one-way time delay and Doppler shift of the channel, while τ_q and ν_q are round-trip time delay and Doppler shift of the target. Consequently, following the procedures in Sections IV-A and IV-B, we can obtain the factor matrices estimation from $\boldsymbol{\mathcal{R}}$, and the leverage the estimated factor matrices to estimate the channel parameters. With these estimated parameters, one can reconstruct the entire THz mMIMO channel matrix $\hat{\mathbf{H}}_{n,k}$. In addition, since the LoS component is predominant in THz bands and the NLoS component experiences significant propagation loss, we can simplify the channel estimation procedure by specifically focusing on estimating channel parameters of the LoS path. This necessitates the estimation of channel parameters with $p = 0$, hence reducing computational overhead while retaining the essential channel state information.

D. Computational Complexity

The computational complexity of the proposed Algorithm 1 is elaborated as follows. Particularly, the complexities associated with computing SVD of $\mathbf{Y}_S$ and EVD of $\mathbf{U}_1^{\dagger}\mathbf{U}_2$ are $\mathcal{O}((K_3N_{\text{tr}})^2L_3M_{\text{re}})$ and $\mathcal{O}(3Q^2K_3N_{\text{tr}}+2Q^3)$, respectively. The complexity of estimating three factor matrices are $\mathcal{O}(QK_{\text{tr}})$, $\mathcal{O}(QK_3N_{\text{tr}}+K_3N_{\text{tr}}^2)$, and $\mathcal{O}(QK_{\text{tr}}N_{\text{tr}}+Q^2K_{\text{tr}}N_{\text{tr}}+QK_{\text{tr}}N_{\text{tr}}M_{\text{re}})$, respectively. Given the number of grid points in the 1-D search as I_{G_θ}, I_{G_τ}, I_{G_ϕ}, and I_{G_ν}, the estimation of $\{\hat{\theta}_q\}_{q=1}^{Q}$, $\{\hat{\tau}_q\}_{q=1}^{Q}$, $\{\phi_q\}_{q=1}^{Q}$, and $\{\nu_q\}_{q=1}^{Q}$ has the complexity order of $\mathcal{O}(QI_{G_\theta}M_{\text{re}})$, $\mathcal{O}(QI_{G_\tau}K_{\text{tr}})$, $\mathcal{O}(QI_{\text{iter}}I_{G_\phi}N_{\text{tr}}N_{\text{bs}})$, and $\mathcal{O}(QI_{\text{iter}}I_{G_\nu}N_{\text{tr}}N_{\text{bs}})$, respectively. The complexity of estimating $\{\beta_q\}_{q=1}^{Q}$ via (37) is $\mathcal{O}(2Q^2K_{\text{tr}}N_{\text{tr}}M_{\text{re}}+Q^3)$. It can observed that the total computational complexity of the proposed algorithm is mainly dependent on the SVD of $\mathbf{Y}_S$ and the estimation of parameters $\{\hat{\theta}_q,\hat{\tau}_q,\hat{\phi}_q,\hat{\nu}_q,\hat{\beta}_q\}_{q=1}^{Q}$.

V. CRB Analysis

In this section, we derive the CRB of estimating the unknown parameters, i.e., $\{\theta_q,\phi_q,\tau_q,\beta_q,\nu_q\}_{q=1}^{Q}$, for the considered problem in (13). Since the CRB characterizes a lower bound on the variance of any unbiased estimator [62], [63], it can behave as a benchmark for evaluating the performance of the proposed algorithm. To be specific, let $\boldsymbol{\xi}$ be a vector stacking all the unknown parameters of interest Q targets, such that $\boldsymbol{\xi}\triangleq[\boldsymbol{\beta}^{\text{T}}\ \boldsymbol{\theta}^{\text{T}}\ \boldsymbol{\phi}^{\text{T}}\ \boldsymbol{\nu}^{\text{T}}\ \boldsymbol{\tau}^{\text{T}}]^{\text{T}}\in\mathbb{C}^{5Q\times 1}$, where $\boldsymbol{\beta}=[\beta_1,\ldots,\beta_Q]^{\text{T}}$, $\boldsymbol{\theta}=[\theta_1,\ldots,\theta_Q]^{\text{T}}$, $\boldsymbol{\phi}=[\phi_1,\ldots,\phi_Q]^{\text{T}}$, $\boldsymbol{\nu}=[\nu_1,\ldots,\nu_Q]^{\text{T}}$, and $\boldsymbol{\tau}=[\tau_1,\ldots,\tau_Q]^{\text{T}}$. We assume that the elements in the noise tensor $\boldsymbol{\mathcal{N}}$ are independent and identically distributed circularly symmetric Gaussian noise with the variance σ^2. Consequently, the log-likelihood function of $\boldsymbol{\xi}$ can be expressed as

$$f(\boldsymbol{\xi})=\text{const}-\frac{1}{\sigma^2}\left\|\mathbf{Y}_{(1)}^{\text{T}}-\left(\mathbf{C}^{(3)}\odot\mathbf{C}^{(2)}\right)\mathbf{C}^{(1)^{\text{T}}}\right\|_F^2 \tag{38}$$

$$=\text{const}-\frac{1}{\sigma^2}\left\|\mathbf{Y}_{(2)}^{\text{T}}-\left(\mathbf{C}^{(3)}\odot\mathbf{C}^{(1)}\right)\mathbf{C}^{(2)^{\text{T}}}\right\|_F^2 \tag{39}$$

$$=\text{const}-\frac{1}{\sigma^2}\left\|\mathbf{Y}_{(3)}^{\text{T}}-\left(\mathbf{C}^{(2)}\odot\mathbf{C}^{(1)}\right)\mathbf{C}^{(3)^{\text{T}}}\right\|_F^2 \tag{40}$$

where $\text{const}=-M_{\text{re}}N_{\text{tr}}K_{\text{tr}}\ln(\pi\sigma^2)$ is defined. Then, the complex Fisher information matrix (FIM) $\boldsymbol{\Omega}(\boldsymbol{\xi})\in\mathbb{C}^{5Q\times 5Q}$ can be calculated as [43]

$$\boldsymbol{\Omega}(\boldsymbol{\xi})=\mathbb{E}\left\{\left(\frac{\partial f(\boldsymbol{\xi})}{\partial\boldsymbol{\xi}}\right)\left(\frac{\partial f(\boldsymbol{\xi})}{\partial\boldsymbol{\xi}}\right)^{H}\right\} \tag{41}$$

and $\boldsymbol{\Omega}(\boldsymbol{\xi})$ for the considered problem is equivalent to the following form with 25 submatrices, i.e.,

$$\boldsymbol{\Omega}(\boldsymbol{\xi})=\begin{bmatrix}\boldsymbol{\Omega}_{\boldsymbol{\beta}\boldsymbol{\beta}} & \boldsymbol{\Omega}_{\boldsymbol{\beta}\boldsymbol{\theta}} & \boldsymbol{\Omega}_{\boldsymbol{\beta}\boldsymbol{\phi}} & \boldsymbol{\Omega}_{\boldsymbol{\beta}\boldsymbol{\nu}} & \boldsymbol{\Omega}_{\boldsymbol{\beta}\boldsymbol{\tau}}\\ \boldsymbol{\Omega}_{\boldsymbol{\beta}\boldsymbol{\theta}}^{H} & \boldsymbol{\Omega}_{\boldsymbol{\theta}\boldsymbol{\theta}} & \boldsymbol{\Omega}_{\boldsymbol{\theta}\boldsymbol{\phi}} & \boldsymbol{\Omega}_{\boldsymbol{\theta}\boldsymbol{\nu}} & \boldsymbol{\Omega}_{\boldsymbol{\theta}\boldsymbol{\tau}}\\ \boldsymbol{\Omega}_{\boldsymbol{\beta}\boldsymbol{\phi}}^{H} & \boldsymbol{\Omega}_{\boldsymbol{\theta}\boldsymbol{\phi}}^{H} & \boldsymbol{\Omega}_{\boldsymbol{\phi}\boldsymbol{\phi}} & \boldsymbol{\Omega}_{\boldsymbol{\phi}\boldsymbol{\nu}} & \boldsymbol{\Omega}_{\boldsymbol{\phi}\boldsymbol{\tau}}\\ \boldsymbol{\Omega}_{\boldsymbol{\beta}\boldsymbol{\nu}}^{H} & \boldsymbol{\Omega}_{\boldsymbol{\theta}\boldsymbol{\nu}}^{H} & \boldsymbol{\Omega}_{\boldsymbol{\phi}\boldsymbol{\nu}}^{H} & \boldsymbol{\Omega}_{\boldsymbol{\nu}\boldsymbol{\nu}} & \boldsymbol{\Omega}_{\boldsymbol{\nu}\boldsymbol{\tau}}\\ \boldsymbol{\Omega}_{\boldsymbol{\beta}\boldsymbol{\tau}}^{H} & \boldsymbol{\Omega}_{\boldsymbol{\theta}\boldsymbol{\tau}}^{H} & \boldsymbol{\Omega}_{\boldsymbol{\phi}\boldsymbol{\tau}}^{H} & \boldsymbol{\Omega}_{\boldsymbol{\nu}\boldsymbol{\tau}}^{H} & \boldsymbol{\Omega}_{\boldsymbol{\tau}\boldsymbol{\tau}}\end{bmatrix} \tag{42}$$

where the detailed derivation of each submatrix can be found in Appendix C. Thereby, the CRB of with respect to the unknown parameters $\boldsymbol{\xi}$ can be obtained by $\text{CRB}(\boldsymbol{\xi})=\boldsymbol{\Omega}^{-1}(\boldsymbol{\xi})$. Since $\boldsymbol{\xi}$ incorporates all the unknown parameters, we can, respectively, obtain the CRB of coefficients, AoAs, AoDs, Doppler shifts, and time delays as follows:

$$\begin{aligned}\text{CRB}(\boldsymbol{\beta})&=\sqrt{\frac{1}{Q}\text{Tr}\left\{\left[\text{CRB}(\boldsymbol{\xi})\right]_{1:Q,1:Q}\right\}}\\ \text{CRB}(\boldsymbol{\theta})&=\sqrt{\frac{1}{Q}\text{Tr}\left\{\left[\text{CRB}(\boldsymbol{\xi})\right]_{Q+1:2Q,Q+1:2Q}\right\}}\\ \text{CRB}(\boldsymbol{\phi})&=\sqrt{\frac{1}{Q}\text{Tr}\left\{\left[\text{CRB}(\boldsymbol{\xi})\right]_{2Q+1:3Q,2Q+1:3Q}\right\}}\\ \text{CRB}(\boldsymbol{\nu})&=\sqrt{\frac{1}{Q}\text{Tr}\left\{\left[\text{CRB}(\boldsymbol{\xi})\right]_{3Q+1:4Q,3Q+1:4Q}\right\}}\\ \text{CRB}(\boldsymbol{\tau})&=\sqrt{\frac{1}{Q}\text{Tr}\left\{\left[\text{CRB}(\boldsymbol{\xi})\right]_{4Q+1:5Q,4Q+1:5Q}\right\}}.\end{aligned} \tag{43}$$

VI. Simulation Results

In this section, we conduct the numerical simulation to investigate the performance of the proposed channel-training-aided target sensing method. We consider a BS equipped with $N_{\text{bs}}=64$ transmit antennas, $N_{\text{re}}=64$ receive antennas, and $N_{\text{ue}}=16$ antennas at the UE. The number of RF chains at the BS and the user side is $M_{\text{re}}=8$, $M_{\text{ue}}=3$ [36]. The carrier frequency is $f_c=0.15$ THz, the bandwidth is $B=500$ MHz with $K=256$, and the CP duration is set to $T_{\text{cp}}=(1/4\Delta f)$ [48]. The power spectral density of the noise is -174 dBm/Hz. The channel coefficients and the target reflection coefficients are generated by [55]

$$\alpha_p=\frac{\lambda_c}{4\pi d_p}e^{j\vartheta_p} \tag{44}$$

$$\beta_q=\sqrt{\frac{\sigma_q\lambda_c^2}{(4\pi)^3d_q^4}}e^{j\vartheta_q} \tag{45}$$

where d_q (d_p) denotes the distance between the ISAC BS and the target (user), σ_q is the RCS of the qth target, ϑ_p and ϑ_q are the corresponding phases and follow from $\mathcal{U}[0,2\pi)$. We set the distance of communication user and the targets distributed $\mathcal{U}[15,30]$ m and $\mathcal{U}[5,15]$ m, respectively. The channel experiences $P=1$ NLoS path and the Rician factor K_{f} is 30 dB. The BS is detecting $Q=6$ targets with RCS being $\sigma_q=1$ m^2. The AoAs and AoDs for either targets or channels are randomly drawn from $[-\pi/3,\pi/3]$. The velocity of each target V_q is uniformly distributed in $[-V_{\max},V_{\max}]$ with the maximum velocity $V_{\max}=15$ m/s. The velocity of the communication user is 20 m/s. For the pilot precoder $\mathbf{P}$ and combiners $\mathbf{W}$ and $\mathbf{Q}$, each element is uniformly drawn from a unit circle [42], and we set $I_{\text{iter}}=30$ and $K_3=K_{\text{tr}}/2$ in Algorithm 1. The target parameters estimation performance is measured by the root-mean-square error (RMSE), i.e., $\text{RMSE}=\sqrt{(1/Q)\sum_{q=1}^{Q}(\hat{\chi}_q-\chi_q)^2}$, where $\hat{\chi}_q$ and χ_q denote the estimated and the corresponding true parameters, respectively, $\chi_q\in\{\theta_q,\phi_q,\tau_q,\nu_q\}$. The target reflection coefficient estimation and the channel estimation performance are evaluated by the normalized-mean-square error (NMSE). In terms of benchmarks for target sensing,

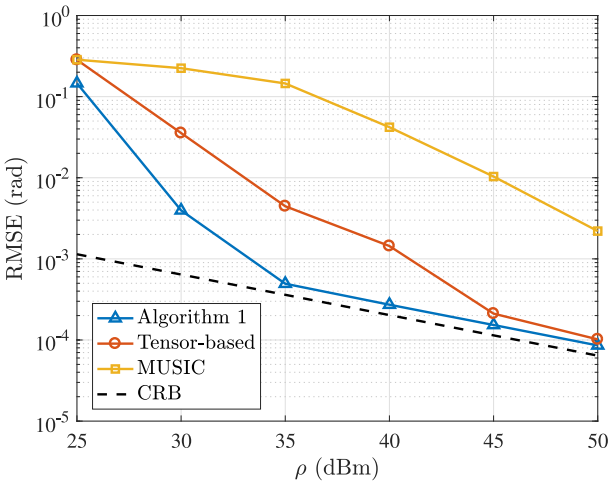

Fig. 2. RMSE performance of AoA estimation versus transmit power.

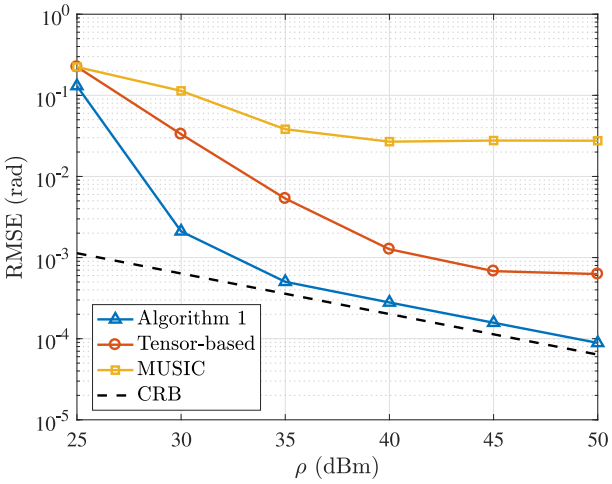

Fig. 3. RMSE performance of AoD estimation versus transmit power.

we employ the multiple signal classification (MUSIC) method for angle estimation and matching filter (MF) algorithm for delay and Doppler estimation [51]. For channel estimation, we employ the CS-based method in [50] for performance comparison. In addition, we employ the conventional tensor-based method employing ALS-based algorithm [42], [43] as the benchmark for both target sensing and channel estimation.

We first investigate the AoA and AoD estimation performance of the proposed Algorithm 1 in Figs. 2 and 3, respectively, where the number of training subcarriers and symbols is set to $K_{\text{tr}} = 64$ and $N_{\text{tr}} = 16$. The estimation results are calculated by taking the average over 95% of the realizations for mitigating the impact of outliers [37]. As observed in Fig. 2, the AoA estimation performance of the proposed Algorithm 1 outperforms both the conventional tensor-based and MUSIC methods, and gradually approaches the CRB as the transmit power increases. Compared to the conventional tensor-based method, the improvement of the proposed Algorithm 1 can be attributed to the factor matrices estimation in Theorem 1, which exploits the Vandermonde structure of the factor matrix. The MUSIC method does not provide satisfactory performance since the training overhead

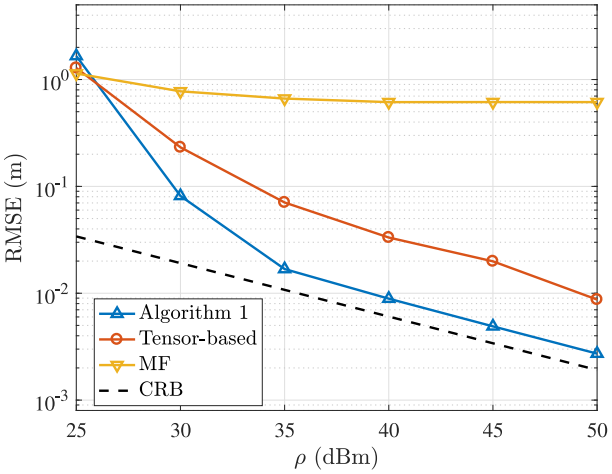

Fig. 4. RMSE performance of range estimation versus transmit power.

in THz-mMIMO-ISAC is limited. In contrast, the proposed Algorithm 1 can capture the intrinsic multidimensional structure of the high-dimensional sensing channel and improve the performance.

In terms of AoD estimation, we can observe from Fig. 3 that the proposed Algorithm 1 can still achieve the superior performance and approach the associated CRB. In contrast, the conventional tensor-based and MUSIC methods encounter the RMSE bottlenecks as the transmit power increases, since they fail to address the coupling problem between the AoD and Doppler shift. This problem is well addressed in the proposed algorithm, where the AoD of targets is iteratively estimated to improve the estimation performance.

Fig. 4 depicts the range estimation performance of the proposed Algorithm 1 as a function of transmit power. It can be observed that the RMSE attained by the proposed Algorithm 1 is better than the benchmarks and is close to the CRB. This is because the proposed Algorithm 1 can independently estimate the time delays of multiple targets from the estimated factor matrices and is free of the grid discretization error. In contrast, the MF-based method requires to discretize the continuous parameter space of time delays into a finite set of grid points, and the grid discretization may limit the parameter estimation performance. To achieve the centimeter-level range estimation performance, the proposed Algorithm 1 only requires 40 dBm of transmit power, while conventional tensor-based method requires more than 50 dBm, significantly saving the system power consumption.

Fig. 5 compares the velocity estimation performance of different benchmarks under the same setting. In this case, the conventional tensor-based method yields the worst RMSE performance of the velocity estimation, since it has no capability to recover the Doppler shift of targets. The MF-based method can attain the improved velocity estimation performance but gradually encounters RMSE performance floor. The proposed Algorithm 1 can achieve the best velocity estimation performance and is close to the corresponding CRB. The performance improvement comes from the iterative estimation of Doppler shifts and AoD, which is consistent with the results in Fig. 3.

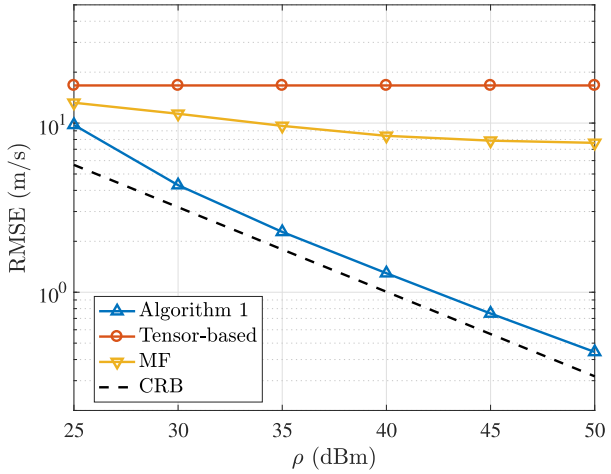

Fig. 5. RMSE performance of velocity estimation versus transmit power.

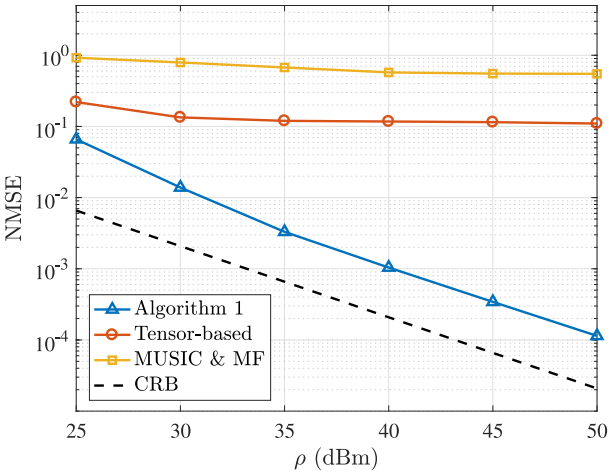

Fig. 6. NMSE performance of target coefficient estimation versus transmit power.

Fig. 6 depicts the NMSE performance of the target reflection coefficients versus transmit power. Note that the estimation of reflection coefficients relies on previous four estimated parameters, i.e., AoA, AoD, range, and velocity. Due to the superior estimation performance of these parameters, the NMSE performance of the proposed Algorithm 1 is best in terms of reflection coefficient estimation and close to its CRB.

Figs. 7 and 8 illustrate the convergence performance of the proposed Algorithm 1 for the estimation of AoD and velocity, respectively, where the RMSE performance is shown as a function of iterations. The number of training subcarriers and symbols is set to $K_{\text{tr}} = 64$ and $N_{\text{tr}} = 16$. We can observe that the AoD estimation performance of the proposed algorithm gradually improves as both the number of iterations and transmit power increases. The similar trend also occurs in terms of the velocity estimation. This means that the proposed algorithm can gradually converge to a stationary solution as the number of iterations increases. To be specific, it takes approximately 30 iterations for convergence in terms of AoD and velocity estimation.

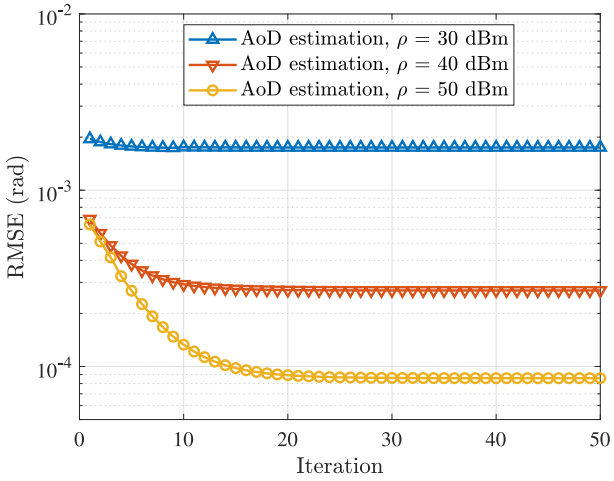

Fig. 7. Convergence performance of the proposed Algorithm 1 for AoD estimation.

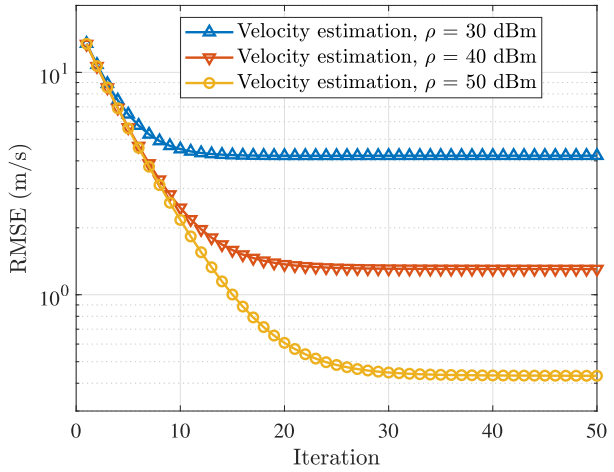

Fig. 8. Convergence performance of the proposed Algorithm 1 for velocity estimation.

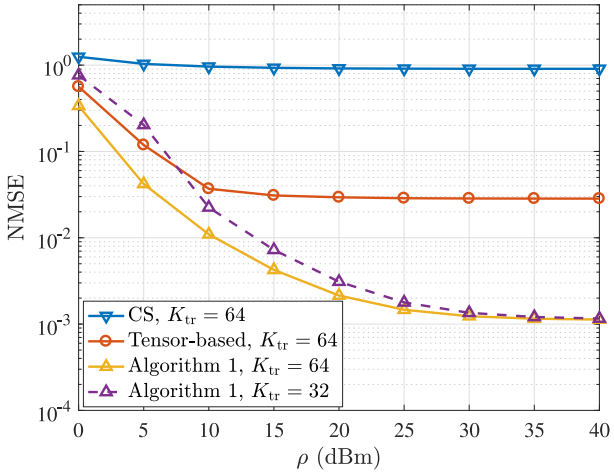

Fig. 9. NMSE performance of channel estimation versus transmit power.

Fig. 9 provides the NMSE performance of the THz mMIMO channel estimation as a function of transmit power. The number of training subcarriers for benchmark methods is $K_{\text{tr}} = 64$ and the proposed algorithm employs $K_{\text{tr}} = 32$

or $K_{\text{tr}} = 64$ training subcarriers. It can be observed that the proposed algorithm yields superior performance with less training overhead. Although the proposed Algorithm 1 only estimates the LoS component of the channel, it still achieves satisfactory channel estimation accuracy. For instance, the estimated NMSE is around 1.4×10^{-3} when the transmit power is only 30 dBm. The performance bottleneck of the proposed Algorithm 1 is because the estimation error caused by NLoS components is dominant at the high transmit power regime. The performance floor of the conventional tensor-based method is more serious due to the ignorance of Doppler effects, which will introduce extra phase distortion accumulation along with channel training. For this issue, the proposed Algorithm 1 can perform the joint estimation of Doppler shift and angle parameters, such that the channel estimation performance can be improved. Note that the CS-based algorithm can not yield satisfactory channel estimation performance, which is caused by the channel time-varying property caused by Doppler effects. In this case, the number of unknown nonzero elements in THz mMIMO channels will increase with channel training, thereby violating the sparsity assumption and degrading the channel estimation performance.

VII. Conclusion

In this article, we proposed a channel-training-aided target sensing framework to facilitate the efficient resource sharing for THz-mMIMO-ISAC. We integrated the target sensing functionality into the channel estimation stage by exploiting the intrinsic connection between the THz mMIMO channel parameters and the target parameters in angular, delay, and Doppler dimensions. Then, a shared channel training pattern accommodating the hybrid architecture constraints of THz transceiver was proposed, such that both the channel estimation and the target sensing can be formulated as two structured tensor decomposition problems at the UE and BS sides, respectively. We proposed a tensor-based algorithm to estimate the parameters, including AoA, AoD, time delays, Doppler shifts, and coefficients, and derived the corresponding CRBs. Numerical results demonstrate that proposed algorithm can achieve the target parameters estimation performance close to their corresponding CRB, and recover the high-dimensional THz mMIMO channels with substantially reduced training overhead.

Appendix A
Preliminaries of Tensor Theory

A. Concepts of Tensor

A tensor is a multidimensional array of numerical values, characterized by its order which denotes the number of dimensions. For instance, a scalar is a zero-order tensor, a vector is a first-order tensor, and a matrix is a second-order tensor. Third-order tensors or higher-order tensors are utilized to represent data with three dimensions or modes, and so forth. Formally, an Nth-order tensor is denoted by $\boldsymbol{\mathcal{X}} \in \mathbb{C}^{I_1 \times I_2 \times \cdots \times I_N}$ with its $(i_1, i_2, \ldots, i_N)$th entry being $\mathcal{X}_{i_1,i_2,\ldots,i_N}$.

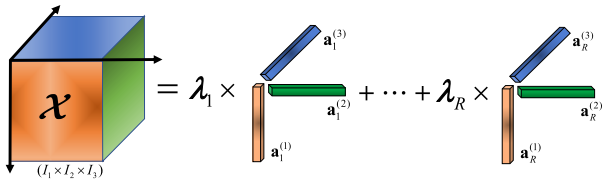

Fig. 10. Diagram of CP decomposition for a third-order tensor $\boldsymbol{\mathcal{X}}$.

B. Definition of Tensor Unfolding

A tensor can be unfolded into a matrix by rearranging its elements. For $\boldsymbol{\mathcal{X}} \in \mathbb{C}^{I_1 \times I_2 \times \cdots \times I_N}$, its mode-$n$ unfolding is denoted by $\mathbf{X}_{(n)} \in \mathbb{C}^{I_n \times \prod_{k \neq n} I_k}$, whose (i_n, j)th element is mapped from $\mathcal{X}_{i_1,i_2,\ldots,i_N}$, $i_n = 1, \ldots, I_n$, and

$$j = 1 + \sum_{\substack{k=1 \\ k \neq n}}^{N} (i_k - 1) J_{k,n}, \; J_{k,n} \triangleq \begin{cases} \prod_{\substack{m=1 \\ m \neq n}}^{k-1} I_m, & \mathcal{I}(k-1) \backslash n \neq \emptyset \\ 1, & \text{otherwise} \end{cases} \tag{46}$$

where $\mathcal{I}(k-1)$ denotes the index set $\{1, 2, \ldots, k-1\}$.

C. Canonical Polyadic Decomposition

Canonical polyadic decomposition (CPD) can factorize an arbitrary tensor into a (weighted) sum of multiple rank-one outer products, i.e.,

$$\boldsymbol{\mathcal{X}} = \sum_{r=1}^{R} \lambda_r \mathbf{a}_r^{(1)} \circ \mathbf{a}_r^{(2)} \circ \cdots \circ \mathbf{a}_r^{(N)} \tag{47}$$

where R is the tensor rank, $\{\lambda_r\}_{r=1}^{R}$ are the weighting coefficients, $\mathbf{a}_r^{(n)} \in \mathbb{C}^{I_n \times 1}$, and $\mathbf{A}^{(n)} \triangleq [\mathbf{a}_1^{(n)}, \ldots, \mathbf{a}_R^{(n)}] \in \mathbb{C}^{I_n \times R}$ is the mode-n factor matrix. For CPD, the mode-n unfolding of $\boldsymbol{\mathcal{X}}$ can be expressed as

$$\mathbf{X}_{(n)} = \mathbf{A}^{(n)} \Xi \left(\mathbf{A}^{(N)} \odot \cdots \odot \mathbf{A}^{(n+1)} \odot \mathbf{A}^{(n-1)} \odot \cdots \odot \mathbf{A}^{(1)} \right)^{\mathrm{T}} \tag{48}$$

where $\Xi \triangleq \text{diag}([\lambda_1, \ldots, \lambda_R])$. As an illustrative example in Fig. 10, we show the CPD of a third-order tensor $\boldsymbol{\mathcal{X}} \in \mathbb{C}^{I_1 \times I_2 \times I_3}$, whose mode-1, mode-2, and mode-3 unfolding are given by $\mathbf{A}^{(1)} \Xi (\mathbf{A}^{(3)} \odot \mathbf{A}^{(2)})^{\mathrm{T}}$, $\mathbf{A}^{(2)} \Xi (\mathbf{A}^{(3)} \odot \mathbf{A}^{(1)})^{\mathrm{T}}$, and $\mathbf{A}^{(3)} \Xi (\mathbf{A}^{(2)} \odot \mathbf{A}^{(1)})^{\mathrm{T}}$, respectively.

Appendix B
Proof of Theorem 1

Proof: To be specific, compute the singular value decomposition $\mathbf{Y}_S = \mathbf{U} \boldsymbol{\Sigma} \mathbf{V}^H = \mathbf{U}_s \boldsymbol{\Sigma}_s \mathbf{V}_s^H + \mathbf{U}_n \boldsymbol{\Sigma}_n \mathbf{V}_n^H$, where the Q principal singular vectors in $\mathbf{U}$ and $\mathbf{V}$ span the signal subspaces $\mathbf{U}_s \in \mathbb{C}^{K_3 N_{\text{tr}} \times Q}$ and $\mathbf{V}_s \in \mathbb{C}^{L_3 M_{\text{re}} \times Q}$, respectively, $\boldsymbol{\Sigma}_s \in \mathbb{C}^{Q \times Q}$ is diagonal matrix formed by the Q largest singular values. Due to the column full rank of $\mathbf{C}^{(K_3,3)} \odot \mathbf{C}^{(2)}$ and $\mathbf{C}^{(1)}$, there must be a nonsingular matrix $\mathbf{M} \in \mathbb{C}^{Q \times Q}$ satisfying

$$\mathbf{U}_s \mathbf{M} = \mathbf{C}^{(K_3,3)} \odot \mathbf{C}^{(2)}. \tag{49}$$

On the other hand, the factor matrix $\mathbf{C}^{(3)}$ exhibits an inherent Vandermonde structure, whose generators are $\{z_{\tau,q} =$

$e^{-j2\pi\tau_q\Delta f}\}_{q=1}^{Q}$. With this structural information, one can verify that for any constant $K_3 \in \{1, 2, \ldots, K_{\text{tr}}\}$, the following equation always holds:

$$\left(\underline{\mathbf{C}}^{(K_3,3)} \odot \mathbf{C}^{(2)}\right)\mathbf{\Lambda} = \left(\overline{\mathbf{C}}^{(K_3,3)} \odot \mathbf{C}^{(2)}\right) \tag{50}$$

where $\underline{\mathbf{C}}^{(K_3,3)} = [\mathbf{C}^{(K_3,3)}]_{1:K_3-1,:} \in \mathbb{C}^{(K_3-1)\times Q}$, $\overline{\mathbf{C}}^{(K_3,3)} = [\mathbf{C}^{(K_3,3)}]_{2:K_3,:} \in \mathbb{C}^{(K_3-1)\times Q}$, $\mathbf{\Lambda} \in \mathbb{C}^{Q\times Q}$ is a diagonal matrix whose qth element being $z_{\tau,q}$. Then, based on (49) and (50), we have

$$\mathbf{U}_1\mathbf{M} = \left(\underline{\mathbf{C}}^{(K_3,3)} \odot \mathbf{C}^{(2)}\right) \tag{51}$$

$$\mathbf{U}_2\mathbf{M} = \left(\overline{\mathbf{C}}^{(K_3,3)} \odot \mathbf{C}^{(2)}\right) \tag{52}$$

where $\mathbf{U}_1$ and $\mathbf{U}_2$ are the submatrices defined by $\mathbf{U}_1 = [\mathbf{U}_s]_{1:(K_3-1)N_{\text{tr}},:}$ and $\mathbf{U}_2 = [\mathbf{U}_s]_{N_{\text{tr}}+1:K_3N_{\text{tr}},:}$, respectively. Accordingly, we have the equivalent form of (50), i.e., $\mathbf{U}_1\mathbf{M}\mathbf{\Lambda} = \mathbf{U}_2\mathbf{M}$. This means that $\mathbf{M}\mathbf{\Lambda}\mathbf{M}^H$ can be regarded as the eigenvalue decomposition of $\mathbf{U}_1^{\dagger}\mathbf{U}_2$, i.e., compute the eigenvalue decomposition as $\mathbf{U}_1^{\dagger}\mathbf{U}_2 = \mathbf{M}\mathbf{\Lambda}\mathbf{M}^H$.

Next, we can obtain the estimated generator as $\hat{z}_{\tau,q} = [\mathbf{\Lambda}]_{q,q}/|[\mathbf{\Lambda}]_{q,q}|$, and $[\mathbf{\Lambda}]_{q,q}$ is the qth diagonal element of $\mathbf{\Lambda}$. Then, the qth column of the factor matrix $\hat{\mathbf{C}}^{(3)}$ can be reconstructed as

$$\hat{\mathbf{c}}_q^{(3)} = \left[\hat{z}_{\tau,q}, \hat{z}_{\tau,q}^2, \ldots, \hat{z}_{\tau,q}^{K_{\text{tr}}}\right]^{\text{T}}. \tag{53}$$

For the qth column of (49), we have

$$\mathbf{c}_q^{(K_3,3)} \otimes \mathbf{c}_q^{(2)} = \mathbf{U}_s\mathbf{m}_q \tag{54}$$

where $\mathbf{m}_q$ is the qth column of $\mathbf{M}$. Following the property of Kronecker product, the qth column of $\hat{\mathbf{C}}^{(2)}$ can be obtained by

$$\begin{aligned}\mathbf{c}_q^{(2)} &= \left(\frac{\mathbf{c}_q^{(K_3,3)H}}{\left\|\mathbf{c}_q^{(K_3,3)}\right\|_2^2} \otimes \mathbf{I}_{N_{\text{tr}}}\right)\left(\mathbf{c}_q^{(K_3,3)} \otimes \mathbf{c}_q^{(2)}\right) \\ &= \left(\frac{\mathbf{c}_q^{(K_3,3)H}}{\left\|\mathbf{c}_q^{(K_3,3)}\right\|_2^2} \otimes \mathbf{I}_{N_{\text{tr}}}\right)\mathbf{U}_s\mathbf{m}_q.\end{aligned} \tag{55}$$

Based on the estimated factor matrices $\hat{\mathbf{C}}^{(3)}$ and $\hat{\mathbf{C}}^{(2)}$, we can turn to estimate $\hat{\mathbf{C}}^{(1)}$ based on (20). By applying the least-squares criterion, we can attain the estimation of $\hat{\mathbf{C}}^{(1)}$ as

$$\hat{\mathbf{C}}^{(1)} = \left(\left(\hat{\mathbf{C}}^{(3)} \odot \hat{\mathbf{C}}^{(2)}\right)^{\dagger}\mathbf{Y}_{(1)}^{\text{T}}\right)^{\text{T}} \tag{56}$$

which completes the proof. ■

APPENDIX C
DERIVATION OF FIM

In this section, we give the derivation of each submatrix in (42), such that CRB can be obtained via (43). We will derive the diagonal submatrices of $\mathbf{\Omega}(\boldsymbol{\xi})$ in first three sections and then derive its off-diagonal submatrices in the remaining sections.

A. Calculation of $\mathbf{\Omega}_{\boldsymbol{\beta}\boldsymbol{\beta}}$

For the FIM submatrix $\mathbf{\Omega}_{\boldsymbol{\beta}\boldsymbol{\beta}} \in \mathbb{C}^{Q\times Q}$, the (q_1, q_2)th entry $[\mathbf{\Omega}_{\boldsymbol{\beta}\boldsymbol{\beta}}]_{q_1,q_2}$ is given by

$$\mathbb{E}\left\{\left(\frac{\partial f(\boldsymbol{\xi})}{\partial \beta_{q_1}}\right)\left(\frac{\partial f(\boldsymbol{\xi})}{\partial \beta_{q_2}}\right)^*\right\}. \tag{57}$$

In (57), the partial derivative of $f(\boldsymbol{\xi})$ with respect to β_q is computed as [42]

$$\frac{\partial f(\boldsymbol{\xi})}{\partial \beta_q} = \text{Tr}\left\{\left(\frac{\partial f(\boldsymbol{\xi})}{\partial \mathbf{C}^{(1)}}\right)^{\text{T}}\frac{\partial \mathbf{C}^{(1)}}{\partial \beta_q} + \left(\frac{\partial f(\boldsymbol{\xi})}{\partial \mathbf{C}^{(1)*}}\right)^{\text{T}}\frac{\partial \mathbf{C}^{(1)*}}{\partial \beta_q}\right\} \tag{58}$$

where each partial derivative is given by

$$\frac{\partial f(\boldsymbol{\xi})}{\partial \mathbf{C}^{(1)}} = \left(\frac{\partial f(\boldsymbol{\xi})}{\partial \mathbf{C}^{(1)*}}\right)^* = \frac{1}{\sigma^2}\mathbf{N}_{(1)}^*\mathbf{C}^{(3,2)} \tag{59}$$

$$\frac{\partial \mathbf{C}^{(1)}}{\partial \beta_q} = \left[\mathbf{0}, \ldots, \mathbf{b}_{\text{re}}(\theta_q), \ldots, \mathbf{0}\right] \in \mathbb{C}^{M_{\text{re}}\times Q} \tag{60}$$

$$\frac{\partial \mathbf{C}^{(1)*}}{\partial \beta_q} = [\mathbf{0}, \ldots, \mathbf{0}, \ldots, \mathbf{0}] \in \mathbb{C}^{M_{\text{re}}\times Q} \tag{61}$$

where $\mathbf{N}_{(1)} = \mathbf{Y}_{(1)} - \mathbf{C}^{(1)}(\mathbf{C}^{(3,2)})^{\text{T}}$is the mode-1 unfolding of the noise tensor $\mathcal{N}$. Then, the partial derivative in (58) can be expressed as $[\partial f(\boldsymbol{\xi})/\partial \beta_q] = \boldsymbol{e}_q^{\text{T}}\mathbf{Z}^{(1)}\boldsymbol{e}_q$, where $\boldsymbol{e}_q$ is the qth column of identity matrix, the term $\mathbf{Z}^{(1)}$ is

$$\mathbf{Z}^{(1)} = \frac{1}{\sigma^2}\left(\mathbf{C}^{(3,2)}\right)^{\text{T}}\mathbf{N}_{(1)}^H\mathbf{B}^{(1)} \tag{62}$$

where $\mathbf{B}^{(1)} = [\mathbf{b}_{\text{re}}(\theta_1), \ldots, \mathbf{b}_{\text{re}}(\theta_Q)]$. Let $\mathbf{z}^{(1)}$ be a vector of $\text{vec}(\mathbf{Z}^{(1)})$, which can be expressed as $\mathbf{z}^{(1)} = (1/\sigma^2)(\mathbf{B}^{(1)^{\text{T}}} \otimes (\mathbf{C}^{(3,2)})^{\text{T}})\text{vec}(\mathbf{N}_{(1)}^H)$, then we can obtain $[\mathbf{\Omega}_{\boldsymbol{\beta}\boldsymbol{\beta}}]_{q_1,q_2}$ as follows:

$$\begin{aligned}\left[\mathbf{\Omega}_{\boldsymbol{\beta}\boldsymbol{\beta}}\right]_{q_1,q_2} &= \mathbb{E}\left\{\left(\mathbf{e}_{q_1}^{\text{T}}\mathbf{Z}^{(1)}\mathbf{e}_{q_1}\right)\left(\mathbf{e}_{q_2}^{\text{T}}\mathbf{Z}^{(1)}\mathbf{e}_{q_2}\right)^*\right\} \\ &= \mathbb{E}\left\{\left[\mathbf{Z}^{(1)}\right]_{q_1,q_1}\left[\mathbf{Z}^{(1)}\right]_{q_2,q_2}^*\right\} \\ &= \mathbb{E}\left\{\left[\mathbf{z}^{(1)}\right]_{l_1}\left[\mathbf{z}^{(1)}\right]_{l_2}^*\right\} = \left[\mathbf{C}_{\mathbf{z}^{(1)}}\right]_{l_1,l_2}\end{aligned} \tag{63}$$

where the third equality follows from $l_1 = Q(q_1-1)+q_1$, $l_2 = Q(q_2-1)+q_2$, and the last equality holds due to the covariance matrix of $\mathbf{z}^{(1)}$ being $\mathbf{C}_{\mathbf{z}^{(1)}} = \mathbb{E}\{(\mathbf{z}^{(1)})(\mathbf{z}^{(1)})^H\}$ and expressed as

$$\begin{aligned}\mathbf{C}_{\mathbf{z}^{(1)}} &= \frac{1}{\sigma^2}\left(\mathbf{B}^{(1)^{\text{T}}} \otimes \left(\mathbf{C}^{(3,2)}\right)^{\text{T}}\right)\left(\mathbf{B}^{(1)*} \otimes \left(\mathbf{C}^{(3,2)}\right)^*\right) \\ &= \frac{1}{\sigma^2}\left(\mathbf{B}^{(1)^{\text{T}}}\mathbf{B}^{(1)*}\right) \otimes \left(\left(\mathbf{C}^{(3,2)}\right)^{\text{T}}\left(\mathbf{C}^{(3,2)}\right)^*\right)\end{aligned} \tag{64}$$

where the second equality exploits the fact $\mathbb{E}\{\text{vec}(\mathbf{N}_{(1)}^H)\text{vec}(\mathbf{N}_{(1)}^H)^H\} = \sigma^2\mathbf{I}_{M_{\text{re}}N_{\text{tr}}K_{\text{tr}}}$ and the last equality holds from the Kronecker product property $(\mathbf{A}_1 \otimes \mathbf{A}_2)(\mathbf{B}_1 \otimes \mathbf{B}_2) = (\mathbf{A}_1\mathbf{B}_1) \otimes (\mathbf{A}_2\mathbf{B}_2)$.

B. Calculation of $\mathbf{\Omega}_{\boldsymbol{\theta}\boldsymbol{\theta}}$

Similarly, to obtain each entry of $\mathbf{\Omega}_{\boldsymbol{\theta}\boldsymbol{\theta}}$, we calculate the partial derivative of $f(\boldsymbol{\xi})$ with respect to θ_q, which is given by

$$\begin{aligned}\frac{\partial f(\boldsymbol{\xi})}{\partial \theta_q} &= \text{Tr}\left\{\left(\frac{\partial f(\boldsymbol{\xi})}{\partial \mathbf{C}^{(1)}}\right)^{\text{T}}\frac{\partial \mathbf{C}^{(1)}}{\partial \theta_q} + \left(\frac{\partial f(\boldsymbol{\xi})}{\partial \mathbf{C}^{(1)*}}\right)^{\text{T}}\frac{\partial \mathbf{C}^{(1)*}}{\partial \theta_q}\right\} \\ &= \boldsymbol{e}_q^{\text{T}}\frac{1}{\sigma^2}\left(\mathbf{C}^{(3,2)}\right)^{\text{T}}\left(\mathbf{Y}_{(1)}^{\text{T}} - \left(\mathbf{C}^{(3,2)}\right)\mathbf{C}^{(1)^{\text{T}}}\right)^*\tilde{\mathbf{B}}^{(1)}\boldsymbol{e}_q\end{aligned}$$

$$+\boldsymbol{e}_q^{\mathrm{T}}\frac{1}{\sigma^2}\left(\mathbf{C}^{(3,2)}\right)^H\left(\mathbf{Y}_{(1)}^{\mathrm{T}}-\left(\mathbf{C}^{(3,2)}\right)\mathbf{C}^{(1)^{\mathrm{T}}}\right)^*\left(\tilde{\mathbf{B}}^{(1)}\right)^*\boldsymbol{e}_q$$
$$=2\mathrm{Re}\left\{\boldsymbol{e}_q^{\mathrm{T}}\frac{1}{\sigma^2}\left(\mathbf{C}^{(3,2)}\right)^{\mathrm{T}}\mathbf{N}_{(1)}^H\tilde{\mathbf{B}}^{(1)}\boldsymbol{e}_q\right\}$$
$$=2\mathrm{Re}\left\{\boldsymbol{e}_q^{\mathrm{T}}\tilde{\mathbf{Z}}^{(1)}\boldsymbol{e}_q\right\} \tag{65}$$

where the second equality holds by defining $\tilde{\mathbf{B}}^{(1)}=[\tilde{\mathbf{b}}_{\mathrm{re},1},\ldots,\tilde{\mathbf{b}}_{\mathrm{re},Q}]$ and the qth column is $\tilde{\mathbf{b}}_{\mathrm{re},q}=-\mathbf{W}^H j\pi\cos(\theta_q)\mathrm{diag}(0,1,\ldots,N_{\mathrm{re}}-1)\mathbf{a}_{\mathrm{re}}(\theta_q)$, the last equality holds by defining

$$\tilde{\mathbf{Z}}^{(1)}=\frac{1}{\sigma^2}\left(\mathbf{C}^{(3,2)}\right)^{\mathrm{T}}\mathbf{N}_{(1)}^H\tilde{\mathbf{B}}^{(1)}. \tag{66}$$

Then, the (q_1,q_2)th entry of $\boldsymbol{\Omega}_{\boldsymbol{\theta\theta}}$ can be expressed as

$$[\boldsymbol{\Omega}_{\boldsymbol{\theta\theta}}]_{q_1,q_2}=\mathbb{E}\left\{\left(\frac{\partial f(\boldsymbol{\xi})}{\partial\theta_{q_1}}\right)\left(\frac{\partial f(\boldsymbol{\xi})}{\partial\theta_{q_2}}\right)^*\right\}$$
$$=4\mathbb{E}\left\{\mathrm{Re}\left\{\mathbf{e}_{q_1}^{\mathrm{T}}\tilde{\mathbf{Z}}^{(1)}\mathbf{e}_{q_1}\right\}\mathrm{Re}\left\{\mathbf{e}_{q_2}^{\mathrm{T}}\tilde{\mathbf{Z}}^{(1)}\mathbf{e}_{q_2}\right\}\right\}$$
$$=\mathbb{E}\left\{\left(\left[\tilde{\mathbf{Z}}^{(1)}\right]_{q_1,q_1}+\left[\tilde{\mathbf{Z}}^{(1)}\right]_{q_1,q_1}^*\right)\left(\left[\tilde{\mathbf{Z}}^{(1)}\right]_{q_2,q_2}+\left[\tilde{\mathbf{Z}}^{(1)}\right]_{q_2,q_2}^*\right)\right\}$$
$$=2\mathrm{Re}\left\{\left[\mathbf{C}_{\tilde{\mathbf{z}}^{(1)}}\right]_{l_1,l_2}\right\}+2\mathrm{Re}\left\{\left[\mathbf{M}_{\tilde{\mathbf{z}}^{(1)}}\right]_{l_1,l_2}\right\} \tag{67}$$

where $\tilde{\mathbf{z}}^{(1)}$ is the vectorization of $\tilde{\mathbf{Z}}^{(1)}$, $\mathbf{C}_{\tilde{\mathbf{z}}^{(1)}}$ is the covariance matrix of $\tilde{\mathbf{z}}^{(1)}$, and $\mathbf{M}_{\tilde{\mathbf{z}}^{(1)}}$ is the pseudo-covariance matrix of $\tilde{\mathbf{z}}^{(1)}$, which are, respectively, given by

$$\tilde{\mathbf{z}}^{(1)}=\frac{1}{\sigma^2}\left(\left(\tilde{\mathbf{B}}^{(1)}\right)^{\mathrm{T}}\otimes\left(\mathbf{C}^{(3,2)}\right)^{\mathrm{T}}\right)\mathrm{vec}\left(\mathbf{N}_{(1)}^{\mathrm{T}}\right) \tag{68}$$
$$\mathbf{C}_{\tilde{\mathbf{z}}^{(1)}}=\mathbb{E}\left\{\left(\tilde{\mathbf{z}}^{(1)}\right)\left(\tilde{\mathbf{z}}^{(1)}\right)^H\right\}$$
$$=\frac{1}{\sigma^2}\left(\left(\tilde{\mathbf{B}}^{(1)}\right)^{\mathrm{T}}\left(\tilde{\mathbf{B}}^{(1)}\right)^*\right)\otimes\left(\left(\mathbf{C}^{(3,2)}\right)^{\mathrm{T}}\left(\mathbf{C}^{(3,2)}\right)^*\right) \tag{69}$$
$$\mathbf{M}_{\tilde{\mathbf{z}}^{(1)}}=\mathbb{E}\left\{\left(\tilde{\mathbf{z}}^{(1)}\right)\left(\tilde{\mathbf{z}}^{(1)}\right)^{\mathrm{T}}\right\}=\mathbf{0}. \tag{70}$$

Accordingly, the FIM submatrix $\boldsymbol{\Omega}_{\boldsymbol{\theta\theta}}$ can be expressed as

$$[\boldsymbol{\Omega}_{\boldsymbol{\theta\theta}}]_{q_1,q_2}=\mathbb{E}\left\{\left(\frac{\partial f(\boldsymbol{\xi})}{\partial\theta_{q_1}}\right)\left(\frac{\partial f(\boldsymbol{\xi})}{\partial\theta_{q_2}}\right)^*\right\}=2\mathrm{Re}\left\{\left[\mathbf{C}_{\tilde{\mathbf{z}}^{(1)}}\right]_{l_1,l_2}\right\}. \tag{71}$$

C. Calculation of $\boldsymbol{\Omega}_{\boldsymbol{\phi\phi}}$, $\boldsymbol{\Omega}_{\boldsymbol{\nu\nu}}$, $\boldsymbol{\Omega}_{\boldsymbol{\tau\tau}}$

Similar to the derivation of $\boldsymbol{\Omega}_{\boldsymbol{\beta\beta}}$ and $\boldsymbol{\Omega}_{\boldsymbol{\theta\theta}}$, we summarize the results of $\boldsymbol{\Omega}_{\boldsymbol{\phi\phi}}$, $\boldsymbol{\Omega}_{\boldsymbol{\nu\nu}}$, and $\boldsymbol{\Omega}_{\boldsymbol{\tau\tau}}$, which are, respectively, given by

$$\left[\boldsymbol{\Omega}_{\boldsymbol{\phi\phi}}\right]_{q_1,q_2}=\mathbb{E}\left\{\left(\frac{\partial f(\boldsymbol{\xi})}{\partial\phi_{q_1}}\right)\left(\frac{\partial f(\boldsymbol{\xi})}{\partial\phi_{q_2}}\right)^*\right\}=2\mathrm{Re}\left\{\left[\mathbf{C}_{\tilde{\mathbf{z}}^{(2)}}\right]_{l_1,l_2}\right\} \tag{72}$$
$$[\boldsymbol{\Omega}_{\boldsymbol{\nu\nu}}]_{q_1,q_2}=\mathbb{E}\left\{\left(\frac{\partial f(\boldsymbol{\xi})}{\partial\nu_{q_1}}\right)\left(\frac{\partial f(\boldsymbol{\xi})}{\partial\nu_{q_2}}\right)^*\right\}=2\mathrm{Re}\left\{\left[\mathbf{C}_{\tilde{\mathbf{z}}^{(2)}}\right]_{l_1,l_2}\right\} \tag{73}$$
$$[\boldsymbol{\Omega}_{\boldsymbol{\tau\tau}}]_{q_1,q_2}=\mathbb{E}\left\{\left(\frac{\partial f(\boldsymbol{\xi})}{\partial\tau_{q_1}}\right)\left(\frac{\partial f(\boldsymbol{\xi})}{\partial\tau_{q_2}}\right)^*\right\}=2\mathrm{Re}\left\{\left[\mathbf{C}_{\tilde{\mathbf{z}}^{(3)}}\right]_{l_1,l_2}\right\} \tag{74}$$

where

$$\mathbf{C}_{\tilde{\mathbf{z}}^{(2)}}=\frac{1}{\sigma^2}\left(\left(\tilde{\mathbf{B}}^{(2)}\right)^{\mathrm{T}}\left(\tilde{\mathbf{B}}^{(2)}\right)^*\right)\otimes\left(\left(\mathbf{C}^{(3,1)}\right)^{\mathrm{T}}\left(\mathbf{C}^{(3,1)}\right)^*\right) \tag{75}$$
$$\mathbf{C}_{\tilde{\mathbf{z}}^{(2)}}=\frac{1}{\sigma^2}\left(\left(\bar{\mathbf{B}}^{(2)}\right)^{\mathrm{T}}\left(\bar{\mathbf{B}}^{(2)}\right)^*\right)\otimes\left(\left(\mathbf{C}^{(3,1)}\right)^{\mathrm{T}}\left(\mathbf{C}^{(3,1)}\right)^*\right) \tag{76}$$
$$\mathbf{C}_{\tilde{\mathbf{z}}^{(3)}}=\frac{1}{\sigma^2}\left(\left(\tilde{\mathbf{B}}^{(3)}\right)^{\mathrm{T}}\left(\tilde{\mathbf{B}}^{(3)}\right)^*\right)\otimes\left(\left(\mathbf{C}^{(2,1)}\right)^{\mathrm{T}}\left(\mathbf{C}^{(2,1)}\right)^*\right) \tag{77}$$

where we define $\mathbf{C}^{(3,1)}=\mathbf{C}^{(3)}\odot\mathbf{C}^{(1)}$, $\mathbf{C}^{(2,1)}=\mathbf{C}^{(2)}\odot\mathbf{C}^{(1)}$, and we introduce the matrices $\tilde{\mathbf{B}}^{(2)}=[\tilde{\mathbf{b}}_{bs,1},\ldots,\tilde{\mathbf{b}}_{\mathrm{bs},Q}]$, $\bar{\mathbf{B}}^{(2)}=[\bar{\mathbf{b}}_{bs,1},\ldots,\bar{\mathbf{b}}_{\mathrm{bs},Q}]$, and $\tilde{\mathbf{B}}^{(3)}=[\tilde{\mathbf{a}}_{td,1},\ldots,\tilde{\mathbf{a}}_{\mathrm{td},Q}]$, whose qth columns are given by

$$\tilde{\mathbf{b}}_{\mathrm{bs},q}=-\boldsymbol{\Gamma}(\nu_q)\mathbf{P}^{\mathrm{T}}j\pi\cos(\phi_q)\mathrm{diag}(0,\ldots,N_{\mathrm{bs}}-1)\mathbf{a}_{\mathrm{bs}}(\phi_q) \tag{78}$$
$$\bar{\mathbf{b}}_{\mathrm{bs},q}=j2\pi T_{\mathrm{sym}}\mathrm{diag}(1,\ldots,N_{\mathrm{tr}})\mathbf{b}_{\mathrm{bs}}(\phi_q,\nu_q) \tag{79}$$
$$\tilde{\mathbf{a}}_{\mathrm{td},q}=-j2\pi\,\mathrm{diag}(\Delta f,2\Delta f,\ldots,K_{\mathrm{tr}}\Delta f)\;\mathbf{a}_{\mathrm{td}}(\tau_q). \tag{80}$$

D. Calculation of $\boldsymbol{\Omega}_{\boldsymbol{\beta\theta}}$

In the following, we give the derivation of off-diagonal submatrices of $\boldsymbol{\Omega}(\boldsymbol{\xi})$. We take $\boldsymbol{\Omega}_{\boldsymbol{\beta\theta}}$ as an example and provide its detailed derivation. To be specific, the (q_1,q_2)th entry of $\Omega_{\boldsymbol{\beta\theta}}$ is given by

$$\left[\boldsymbol{\Omega}_{\boldsymbol{\beta\theta}}\right]_{q_1,q_2}=\mathbb{E}\left\{\left(\frac{\partial f(\boldsymbol{\xi})}{\partial\beta_{q_1}}\right)\left(\frac{\partial f(\boldsymbol{\xi})}{\partial\theta_{q_2}}\right)^*\right\}$$
$$=\mathbb{E}\left\{\left(\mathbf{e}_{q_1}^{\mathrm{T}}\mathbf{Z}^{(1)}\mathbf{e}_{q_1}\right)\left(\mathbf{e}_{q_2}^{\mathrm{T}}\tilde{\mathbf{Z}}^{(1)}\mathbf{e}_{q_2}\right)^*\right\}$$
$$=\mathbb{E}\left\{\left[\mathbf{Z}^{(1)}\right]_{q_1,q_1}\left[\tilde{\mathbf{Z}}^{(1)}\right]_{q_2,q_2}^*\right\}=\left[\mathbf{C}_{\mathbf{z}^{(1)},\tilde{\mathbf{z}}^{(1)}}\right]_{l_1,l_2} \tag{81}$$

where the second equality holds by exploiting the expression of (58) and (65), $l_1=Q(q_1-1)+q_1$, $l_2=Q(q_2-1)+q_2$, and the last equality holds due to the equivalence of $\mathbb{E}\{[\mathbf{Z}^{(1)}]_{q_1,q_1}[\tilde{\mathbf{Z}}^{(1)}]_{q_2,q_2}^*\}$ to the (l_1,l_2)th entry of the cross-covariance matrix $\mathbf{C}_{\mathbf{z}^{(1)},\tilde{\mathbf{z}}^{(1)}}$, which is expressed as

$$\mathbf{C}_{\mathbf{z}^{(1)},\tilde{\mathbf{z}}^{(1)}}=\mathbb{E}\left\{\left(\mathbf{z}^{(1)}\right)\left(\tilde{\mathbf{z}}^{(1)}\right)^H\right\}$$
$$=\frac{1}{\sigma^2}\left(\left(\mathbf{B}^{(1)}\right)^{\mathrm{T}}\otimes\left(\mathbf{C}^{(3,2)}\right)^{\mathrm{T}}\right)\left(\left(\tilde{\mathbf{B}}^{(1)}\right)^*\otimes\left(\mathbf{C}^{(3,2)}\right)^*\right)$$
$$=\frac{1}{\sigma^2}\left(\mathbf{B}^{(1)}\otimes\mathbf{C}^{(3,2)}\right)^{\mathrm{T}}\left(\tilde{\mathbf{B}}^{(1)}\otimes\mathbf{C}^{(3,2)}\right)^* \tag{82}$$

where the second equality exploits the covariance matrix of $\mathrm{vec}(\mathbf{N}_{(1)}^H)$ and the Kronecker product property.

E. Calculation of $\boldsymbol{\Omega}_{\boldsymbol{\theta\phi}}$

For the FIM submatrix $\boldsymbol{\Omega}_{\boldsymbol{\theta\phi}}$, the (q_1,q_2)th entry is given by

$$\left[\boldsymbol{\Omega}_{\boldsymbol{\theta\phi}}\right]_{q_1,q_2}=\mathbb{E}\left\{\left(\frac{\partial f(\boldsymbol{\xi})}{\partial\theta_{q_1}}\right)\left(\frac{\partial f(\boldsymbol{\xi})}{\partial\phi_{q_2}}\right)^*\right\}$$
$$=4\mathbb{E}\left\{\mathrm{Re}\left\{\mathbf{e}_{q_1}^{\mathrm{T}}\tilde{\mathbf{Z}}^{(1)}\mathbf{e}_{q_1}\right\}\mathrm{Re}\left\{\mathbf{e}_{q_2}^{\mathrm{T}}\tilde{\mathbf{Z}}^{(2)}\mathbf{e}_{q_2}\right\}^*\right\}$$
$$=\mathbb{E}\left\{\left(\left[\tilde{\mathbf{Z}}^{(1)}\right]_{q_1,q_1}+\left[\tilde{\mathbf{Z}}^{(1)}\right]_{q_1,q_1}^*\right)\left(\left[\tilde{\mathbf{Z}}^{(2)}\right]_{q_2,q_2}+\left[\tilde{\mathbf{Z}}^{(2)}\right]_{q_2,q_2}^*\right)\right\}$$
$$=2\mathrm{Re}\left\{\left[\mathbf{C}_{\tilde{\mathbf{z}}^{(1)},\tilde{\mathbf{z}}^{(2)}}\right]_{l_1,l_2}\right\}+2\mathrm{Re}\left\{\left[\mathbf{M}_{\tilde{\mathbf{z}}^{(1)},\tilde{\mathbf{z}}^{(2)}}\right]_{l_1,l_2}\right\} \tag{83}$$

where the equalities holds by exploiting the known results in (65) and (72). In (83), the pseudo-cross-covariance matrix $\mathbf{M}_{\tilde{\mathbf{z}}^{(1)},\tilde{\mathbf{z}}^{(2)}}=\mathbf{0}$, and the cross-covariance matrix is

$$\mathbf{C}_{\tilde{\mathbf{z}}^{(1)},\tilde{\mathbf{z}}^{(2)}}=\mathbb{E}\left\{\left(\tilde{\mathbf{z}}^{(1)}\right)\left(\tilde{\mathbf{z}}^{(2)}\right)^H\right\}$$
$$=\frac{1}{\sigma^4}\left(\tilde{\mathbf{B}}^{(1)}\otimes\mathbf{C}^{(3,2)}\right)^{\mathrm{T}}\mathbf{C}_{\mathbf{n}_1,\mathbf{n}_2}\left(\tilde{\mathbf{B}}^{(2)}\otimes\mathbf{C}^{(3,1)}\right)^* \tag{84}$$

where $\mathbf{C}_{\mathbf{n}_1,\mathbf{n}_2} \triangleq \mathbb{E}\{\text{vec}(\mathbf{N}_{(1)}^H)\text{vec}(\mathbf{N}_{(2)}^H)^H\} \in \mathbb{C}^{M_{\text{re}}N_{\text{tr}}K_{\text{tr}} \times M_{\text{re}}N_{\text{tr}}K_{\text{tr}}}$ is the cross-covariance matrix of the noise term. To calculate $\mathbf{C}_{\mathbf{n}_1,\mathbf{n}_2}$, we notice that the (m,n,k)th entry of the noise tensor $\mathcal{N} \in \mathbb{C}^{M_{\text{re}} \times N_{\text{tr}} \times K_{\text{tr}}}$ can be expressed as either the $(n+(k-1)N_{\text{tr}} +(m-1)N_{\text{tr}}K_{\text{tr}})$th entry of $\text{vec}(\mathbf{N}_{(1)}^H)$ or the $(m+(k-1)M_{\text{re}} +(n-1)M_{\text{re}}K_{\text{tr}})$th entry of $\text{vec}(\mathbf{N}_{(2)}^H)$ [43]. Since the elements in $\mathcal{N}$ follow from $\mathcal{CN}(0,\sigma^2)$, we can compute $\mathbf{C}_{\mathbf{n}_1,\mathbf{n}_2}$ as

$$\begin{aligned}\mathbf{C}_{\mathbf{n}_1,\mathbf{n}_2} &= \mathbb{E}\left\{\text{vec}\left(\mathbf{N}_{(1)}^H\right)\text{vec}\left(\mathbf{N}_{(2)}^H\right)^H\right\} \\ &= \sigma^2 \sum_{m=1}^{M_{\text{re}}}\sum_{n=1}^{N_{\text{tr}}}\sum_{k=1}^{K_{\text{tr}}} \mathbf{e}_{n+(k-1)N_{\text{tr}}+(m-1)N_{\text{tr}}K_{\text{tr}}} \\ &\quad \cdot \mathbf{e}_{m+(k-1)M_{\text{re}}+(n-1)M_{\text{re}}K_{\text{tr}}}^{\text{T}} \end{aligned} \tag{85}$$

where only $M_{\text{re}}N_{\text{tr}}K_{\text{tr}}$ entries in $\mathbf{C}_{\mathbf{n}_1,\mathbf{n}_2}$ are nonzero. In addition, we can calculate

$$\begin{aligned}\mathbf{C}_{\mathbf{n}_1,\mathbf{n}_3} &= \sigma^2 \sum_{m=1}^{M_{\text{re}}}\sum_{n=1}^{N_{\text{tr}}}\sum_{k=1}^{K_{\text{tr}}} \mathbf{e}_{n+(k-1)N_{\text{tr}}+(m-1)N_{\text{tr}}K_{\text{tr}}} \\ &\quad \cdot \mathbf{e}_{m+(t-1)M_{\text{re}}+(k-1)M_{\text{re}}N_{\text{tr}}}^{\text{T}} \end{aligned} \tag{86}$$

$$\begin{aligned}\mathbf{C}_{\mathbf{n}_2,\mathbf{n}_3} &= \sigma^2 \sum_{m=1}^{M_{\text{re}}}\sum_{n=1}^{N_{\text{tr}}}\sum_{k=1}^{K_{\text{tr}}} \mathbf{e}_{m+(k-1)M_{\text{re}}+(n-1)M_{\text{re}}K_{\text{tr}}} \\ &\quad \cdot \mathbf{e}_{m+(t-1)M_{\text{re}}+(k-1)M_{\text{re}}N_{\text{tr}}}^{\text{T}}. \end{aligned} \tag{87}$$

F. Calculation of Other Off-Principal Submatrices

Similar to the derivation in previous sections, we summarize the results of remaining FIM submatrices. They are summarized as follows:

$$\left[\boldsymbol{\Omega}_{\boldsymbol{\beta}\boldsymbol{\phi}}\right]_{q_1,q_2} = \left[\mathbf{C}_{\mathbf{z}^{(1)},\tilde{\mathbf{z}}^{(2)}}\right]_{l_1,l_2} \tag{88}$$

$$\left[\boldsymbol{\Omega}_{\boldsymbol{\beta}\boldsymbol{\nu}}\right]_{q_1,q_2} = \left[\mathbf{C}_{\mathbf{z}^{(1)},\bar{\mathbf{z}}^{(2)}}\right]_{l_1,l_2} \tag{89}$$

$$\left[\boldsymbol{\Omega}_{\boldsymbol{\beta}\boldsymbol{\tau}}\right]_{q_1,q_2} = \left[\mathbf{C}_{\mathbf{z}^{(1)},\tilde{\mathbf{z}}^{(3)}}\right]_{l_1,l_2} \tag{90}$$

$$\left[\boldsymbol{\Omega}_{\boldsymbol{\theta}\boldsymbol{\nu}}\right]_{q_1,q_2} = 2\text{Re}\left\{\left[\mathbf{C}_{\tilde{\mathbf{z}}^{(1)},\bar{\mathbf{z}}^{(2)}}\right]_{l_1,l_2}\right\} \tag{91}$$

$$\left[\boldsymbol{\Omega}_{\boldsymbol{\theta}\boldsymbol{\tau}}\right]_{q_1,q_2} = 2\text{Re}\left\{\left[\mathbf{C}_{\tilde{\mathbf{z}}^{(1)},\tilde{\mathbf{z}}^{(3)}}\right]_{l_1,l_2}\right\} \tag{92}$$

$$\left[\boldsymbol{\Omega}_{\boldsymbol{\phi}\boldsymbol{\nu}}\right]_{q_1,q_2} = 2\text{Re}\left\{\left[\mathbf{C}_{\tilde{\mathbf{z}}^{(2)},\bar{\mathbf{z}}^{(2)}}\right]_{l_1,l_2}\right\} \tag{93}$$

$$\left[\boldsymbol{\Omega}_{\boldsymbol{\phi}\boldsymbol{\tau}}\right]_{q_1,q_2} = 2\text{Re}\left\{\left[\mathbf{C}_{\tilde{\mathbf{z}}^{(2)},\tilde{\mathbf{z}}^{(3)}}\right]_{l_1,l_2}\right\} \tag{94}$$

$$\left[\boldsymbol{\Omega}_{\boldsymbol{\nu}\boldsymbol{\tau}}\right]_{q_1,q_2} = 2\text{Re}\left\{\left[\mathbf{C}_{\bar{\mathbf{z}}^{(2)},\tilde{\mathbf{z}}^{(3)}}\right]_{l_1,l_2}\right\} \tag{95}$$

where the cross-covariance matrices are given by

$$\mathbf{C}_{\mathbf{z}^{(1)},\tilde{\mathbf{z}}^{(2)}} = \frac{1}{\sigma^4}\left(\mathbf{B}^{(1)} \otimes \mathbf{C}^{(3,2)}\right)^{\text{T}}\mathbf{C}_{\mathbf{n}_1,\mathbf{n}_2}\left(\tilde{\mathbf{B}}^{(2)} \otimes \mathbf{C}^{(3,1)}\right)^* \tag{96}$$

$$\mathbf{C}_{\mathbf{z}^{(1)}\bar{\mathbf{z}}^{(2)}} = \frac{1}{\sigma^4}\left(\mathbf{B}^{(1)} \otimes \mathbf{C}^{(3,2)}\right)^{\text{T}}\mathbf{C}_{\mathbf{n}_1,\mathbf{n}_2}\left(\bar{\mathbf{B}}^{(2)} \otimes \mathbf{C}^{(3,1)}\right)^* \tag{97}$$

$$\mathbf{C}_{\mathbf{z}^{(1)},\tilde{\mathbf{z}}^{(3)}} = \frac{1}{\sigma^4}\left(\mathbf{B}^{(1)} \otimes \mathbf{C}^{(3,2)}\right)^{\text{T}}\mathbf{C}_{\mathbf{n}_1,\mathbf{n}_3}\left(\tilde{\mathbf{B}}^{(3)} \otimes \mathbf{C}^{(2,1)}\right)^* \tag{98}$$

$$\mathbf{C}_{\tilde{\mathbf{z}}^{(1)},\bar{\mathbf{z}}^{(2)}} = \frac{1}{\sigma^4}\left(\tilde{\mathbf{B}}^{(1)} \otimes \mathbf{C}^{(3,2)}\right)^{\text{T}}\mathbf{C}_{\mathbf{n}_1,\mathbf{n}_2}\left(\bar{\mathbf{B}}^{(2)} \otimes \mathbf{C}^{(3,1)}\right)^* \tag{99}$$

$$\mathbf{C}_{\tilde{\mathbf{z}}^{(1)},\tilde{\mathbf{z}}^{(3)}} = \frac{1}{\sigma^4}\left(\tilde{\mathbf{B}}^{(1)} \otimes \mathbf{C}^{(3,2)}\right)^{\text{T}}\mathbf{C}_{\mathbf{n}_1,\mathbf{n}_3}\left(\tilde{\mathbf{B}}^{(3)} \otimes \mathbf{C}^{(2,1)}\right)^* \tag{100}$$

$$\mathbf{C}_{\tilde{\mathbf{z}}^{(2)},\tilde{\mathbf{z}}^{(2)}} = \frac{1}{\sigma^2}\left(\tilde{\mathbf{B}}^{(2)} \otimes \mathbf{C}^{(3,1)}\right)^{\text{T}}\left(\bar{\mathbf{B}}^{(2)} \otimes \mathbf{C}^{(3,1)}\right)^* \tag{101}$$

$$\mathbf{C}_{\tilde{\mathbf{z}}^{(2)},\tilde{\mathbf{z}}^{(3)}} = \frac{1}{\sigma^4}\left(\tilde{\mathbf{B}}^{(2)} \otimes \mathbf{C}^{(3,2)}\right)^{\text{T}}\mathbf{C}_{\mathbf{n}_2,\mathbf{n}_3}\left(\tilde{\mathbf{B}}^{(3)} \otimes \mathbf{C}^{(2,1)}\right)^* \tag{102}$$

$$\mathbf{C}_{\bar{\mathbf{z}}^{(2)},\tilde{\mathbf{z}}^{(3)}} = \frac{1}{\sigma^4}\left(\bar{\mathbf{B}}^{(2)} \otimes \mathbf{C}^{(3,2)}\right)^{\text{T}}\mathbf{C}_{\mathbf{n}_2,\mathbf{n}_3}\left(\tilde{\mathbf{B}}^{(3)} \otimes \mathbf{C}^{(2,1)}\right)^*. \tag{103}$$

REFERENCES

[1] Y. Cui, F. Liu, X. Jing, and J. Mu, "Integrating sensing and communications for ubiquitous IoT: Applications, trends, and challenges," *IEEE Netw.*, vol. 35, no. 5, pp. 158–167, Sep./Oct. 2021.

[2] F. Liu et al., "Integrated sensing and communications: Toward dual-functional wireless networks for 6G and beyond," *IEEE J. Sel. Areas Commun.*, vol. 40, no. 6, pp. 1728–1767, Jun. 2022.

[3] B. Yu, Y. Cai, D. Wu, C. Dong, R. Zhang, and W. Wu, "Optimizing age of information for uplink cellular internet of things with random access," *IEEE Internet Things J.*, vol. 11, no. 11, pp. 20300–20313, Jun. 2024.

[4] W. Zhou, R. Zhang, G. Chen, and W. Wu, "Integrated sensing and communication waveform design: A survey," *IEEE Open J. Commun. Soc.*, vol. 3, pp. 1930–1949, 2022.

[5] A. Liu et al., "A survey on fundamental limits of integrated sensing and communication," *IEEE Commun. Surveys Tuts.*, vol. 24, no. 2, pp. 994–1034, 2nd Quart., 2022.

[6] X. Gan et al., "Coverage and rate analysis for integrated sensing and communication networks," *IEEE J. Sel. Areas Commun.*, vol. 42, no. 9, pp. 2213–2227, Sep. 2024.

[7] C.-X. Wang, J. Wang, S. Hu, Z. H. Jiang, J. Tao, and F. Yan, "Key technologies in 6G terahertz wireless communication systems: A survey," *IEEE Veh. Technol. Mag.*, vol. 16, no. 4, pp. 27–37, Dec. 2021.

[8] E. G. Larsson, O. Edfors, F. Tufvesson, and T. L. Marzetta, "Massive MIMO for next generation wireless systems," *IEEE Commun. Mag.*, vol. 52, no. 2, pp. 186–195, Feb. 2014.

[9] A. Faisal, H. Sarieddeen, H. Dahrouj, T. Y. Al-Naffouri, and M.-S. Alouini, "Ultramassive MIMO systems at terahertz bands: Prospects and challenges," *IEEE Veh. Technol. Mag.*, vol. 15, no. 4, pp. 33–42, Dec. 2020.

[10] H. Sarieddeen, N. Saeed, T. Y. Al-Naffouri, and M.-S. Alouini, "Next generation terahertz communications: A rendezvous of sensing, imaging, and localization," *IEEE Commun. Mag.*, vol. 58, no. 5, pp. 69–75, May 2020.

[11] Z. Chen et al., "Terahertz wireless communications for 2030 and beyond: A cutting-edge frontier," *IEEE Commun. Mag.*, vol. 59, no. 11, pp. 66–72, Nov. 2021.

[12] C. Jiang, C. Zhang, C. Huang, J. Ge, J. He, and C. Yuen, "Secure beamforming design for RIS-assisted integrated sensing and communication systems," *IEEE Wireless Commun. Lett.*, vol. 13, no. 2, pp. 520–524, Feb. 2024.

[13] H. Sarieddeen, M.-S. Alouini, and T. Y. Al-Naffouri, "An overview of signal processing techniques for terahertz communications," *Proc. IEEE*, vol. 109, no. 10, pp. 1628–1665, Oct. 2021.

[14] D. Li, "How many reflecting elements are needed for energy- and spectral-efficient intelligent reflecting surface-assisted communication," *IEEE Trans. Commun.*, vol. 70, no. 2, pp. 1320–1331, Feb. 2022.

[15] P. Stoica and A. Nehorai, "MUSIC, maximum likelihood, and Cramer–Rao bound," *IEEE Trans. Acoust., Speech, Signal Process.*, vol. 37, no. 5, pp. 720–741, May 1989.

[16] H. Krim and M. Viberg, "Two decades of array signal processing research: The parametric approach," *IEEE Signal Process. Mag.*, vol. 13, no. 4, pp. 67–94, Jul. 1996.

[17] L. Xu, J. Li, and P. Stoica, "Target detection and parameter estimation for MIMO radar systems," *IEEE Trans. Aerosp. Election. Syst.*, vol. 44, no. 3, pp. 927–939, Jul. 2008.

[18] C. Sturm and W. Wiesbeck, "Waveform design and signal processing aspects for fusion of wireless communications and radar sensing," *Proc. IEEE*, vol. 99, no. 7, pp. 1236–1259, Jul. 2011.

[19] M. L. Rahman, J. A. Zhang, X. Huang, Y. J. Guo, and R. W. Heath, "Framework for a perceptive mobile network using joint communication and radar sensing," *IEEE Trans. Aerosp. Electron. Syst.*, vol. 56, no. 3, pp. 1926–1941, Jun. 2020.

[20] M. F. Keskin, H. Wymeersch, and V. Koivunen, "MIMO-OFDM joint radar-communications: Is ICI friend or foe?" *IEEE J. Sel. Topics Signal Process.*, vol. 15, no. 6, pp. 1393–1408, Nov. 2021.

[21] R. Zhang, B. Shim, W. Yuan, M. D. Renzo, X. Dang, and W. Wu, "Integrated sensing and communication waveform design with sparse vector coding: Low sidelobes and ultra reliability," *IEEE Trans. Veh. Technol.*, vol. 71, no. 4, pp. 4489–4494, Apr. 2022.

[22] Z. Wei et al., "Carrier aggregation enabled integrated sensing and communication signal design and processing," *IEEE Trans. Veh. Technol.*, vol. 73, no. 3, pp. 3580–3596, Mar. 2024.
[23] X. Gan et al., "Bayesian learning for double-RIS aided ISAC systems with superimposed pilots and data," *IEEE J. Sel. Topics Signal Process.*, early access, May 31, 2024, doi: 10.1109/JSTSP.2024.3408071.
[24] W. Lyu et al., "CRB minimization for RIS-aided mmWave integrated sensing and communications," *IEEE Internet Things J.*, vol. 11, no. 10, pp. 18381–18393, May 2024.
[25] J. Zhang et al., "Joint design for STAR-RIS aided ISAC: Decoupling or learning," *IEEE Trans. Wireless Commun.*, early access, Jun. 19, 2024, doi: 10.1109/TWC.2024.3413089.
[26] J. Zhang, J. Xu, W. Lu, N. Zhao, X. Wang, and D. Niyato, "Secure transmission for IRS-aided UAV-ISAC networks," *IEEE Trans. Wireless Commun.*, early access, Apr. 24, 2024, doi: 10.1109/TWC.2024.3390169.
[27] T. Mao, J. Chen, Q. Wang, C. Han, Z. Wang, and G. K. Karagiannidis, "Waveform design for joint sensing and communications in millimeter-wave and low terahertz bands," *IEEE Trans. Commun.*, vol. 70, no. 10, pp. 7023–7039, Oct. 2022.
[28] Y. Wu, F. Lemic, C. Han, and Z. Chen, "Sensing integrated DFT-spread OFDM waveform and deep learning-powered receiver design for terahertz integrated sensing and communication systems," *IEEE Trans. Commun.*, vol. 71, no. 1, pp. 595–610, Jan. 2023.
[29] H. Sarieddeen, M.-S. Alouini, and T. Y. Al-Naffouri, "Terahertz-band ultra-massive spatial modulation MIMO," *IEEE J. Sel. Areas Commun.*, vol. 37, no. 9, pp. 2040–2052, Sep. 2019.
[30] A. Hassanien and S. A. Vorobyov, "Phased-MIMO radar: A tradeoff between phased-array and MIMO radars," *IEEE Trans. Signal Process.*, vol. 58, no. 6, pp. 3137–3151, Jun. 2010.
[31] F. Gao, B. Wang, C. Xing, J. An, and G. Y. Li, "Wideband beamforming for hybrid massive MIMO terahertz communications," *IEEE J. Sel. Areas Commun.*, vol. 39, no. 6, pp. 1725–1740, Jun. 2021.
[32] C. Han, L. Yan, and J. Yuan, "Hybrid beamforming for terahertz wireless communications: Challenges, architectures, and open problems," *IEEE Wireless Commun.*, vol. 28, no. 4, pp. 198–204, Apr. 2021.
[33] Z. Cheng, Z. He, and B. Liao, "Hybrid beamforming design for OFDM dual-function radar-communication system," *IEEE J. Sel. Topics Signal Process.*, vol. 15, no. 6, pp. 1455–1467, Nov. 2021.
[34] R. Zhang, B. Shim, and W. Wu, "Direction-of-arrival estimation for large antenna arrays with hybrid analog and digital architectures," *IEEE Trans. Signal Process.*, vol. 70, pp. 72–88, Jan. 2022.
[35] F. Gao, L. Xu, and S. Ma, "Integrated sensing and communications with joint beam-squint and beam-split for mmWave/THz massive MIMO," *IEEE Trans. Commun.*, vol. 71, no. 5, pp. 2963–2976, May 2023.
[36] K. Venugopal, A. Alkhateeb, N. G. Prelcic, and R. W. Heath, "Channel estimation for hybrid architecture-based wideband millimeter wave systems," *IEEE J. Sel. Areas Commun.*, vol. 35, no. 9, pp. 1996–2009, Sep. 2017.
[37] N. J. Myers and R. W. Heath, "Message passing-based joint CFO and channel estimation in mmWave systems with one-bit ADCs," *IEEE Trans. Wireless Commun.*, vol. 18, no. 6, pp. 3064–3077, Jun. 2019.
[38] R. Zhang, B. Shim, and H. Zhao, "Downlink compressive channel estimation with phase noise in massive MIMO systems," *IEEE Trans. Commun.*, vol. 68, no. 9, pp. 5534–5548, Sep. 2020.
[39] R. Zhang, J. Zhang, T. Zhao, and H. Zhao, "Block sparse recovery for wideband channel estimation in hybrid mmWave MIMO systems," in *Proc. IEEE Glob. Commun. Conf. (GLOBECOM)*, 2018, pp. 1–6.
[40] M. Wang, F. Gao, N. Shlezinger, M. F. Flanagan, and Y. C. Eldar, "A block sparsity based estimator for mmWave massive MIMO channels with beam squint," *IEEE Trans. Signal Process.*, vol. 68, pp. 49–64, Jan. 2020.
[41] S. Gao, X. Cheng, and L. Yang, "Estimating doubly-selective channels for hybrid mmWave massive MIMO systems: A doubly-sparse approach," *IEEE Trans. Wireless Commun.*, vol. 19, no. 9, pp. 5703–5715, Sep. 2020.
[42] Z. Zhou, J. Fang, L. Yang, H. Li, Z. Chen, and R. S. Blum, "Low-rank tensor decomposition-aided channel estimation for millimeter wave MIMO-OFDM systems," *IEEE J. Sel. Areas Commun.*, vol. 35, no. 7, pp. 1524–1538, Jul. 2017.
[43] S. Park, A. Ali, N. González-Prelcic, and R. W. Heath, "Spatial channel covariance estimation for hybrid architectures based on tensor decompositions," *IEEE Trans. Wireless Commun.*, vol. 19, no. 2, pp. 1084–1097, Feb. 2020.
[44] C. Qian, X. Fu, and N. D. Sidiropoulos, "Algebraic channel estimation algorithms for FDD massive MIMO systems," *IEEE J. Sel. Topics Signal Process.*, vol. 13, no. 5, pp. 961–973, Sep. 2019.
[45] Y. Lin, S. Jin, M. Matthaiou, and X. You, "Tensor-based channel estimation for millimeter wave MIMO-OFDM with dual-wideband effects," *IEEE Trans. Commun.*, vol. 68, no. 7, pp. 4218–4232, Jul. 2020.
[46] R. Zhang, L. Cheng, S. Wang, Y. Lou, W. Wu, and D. W. K. Ng, "Tensor decomposition-based channel estimation for hybrid mmWave massive MIMO in high-mobility scenarios," *IEEE Trans. Commun.*, vol. 70, no. 9, pp. 6325–6340, Sep. 2022.
[47] C. Han et al., "Terahertz wireless channels: A holistic survey on measurement, modeling, and analysis," *IEEE Commun. Surveys Tuts.*, vol. 24, no. 3, pp. 1670–1707, 3rd Quart., 2022.
[48] Z. Wan, Z. Gao, F. Gao, M. D. Renzo, and M.-S. Alouini, "Terahertz massive MIMO with holographic reconfigurable intelligent surfaces," *IEEE Trans. Commun.*, vol. 69, no. 7, pp. 4732–4750, Jul. 2021.
[49] X. Gao, L. Dai, Y. Zhang, T. Xie, X. Dai, and Z. Wang, "Fast channel tracking for terahertz beamspace massive MIMO systems," *IEEE Trans. Veh. Technol.*, vol. 66, no. 7, pp. 5689–5696, Jul. 2017.
[50] K. Dovelos, M. Matthaiou, H. Q. Ngo, and B. Bellalta, "Channel estimation and hybrid combining for wideband terahertz massive MIMO systems," *IEEE J. Sel. Areas Commun.*, vol. 39, no. 6, pp. 1604–1620, Jun. 2021.
[51] F. Liu, C. Masouros, A. P. Petropulu, H. Griffiths, and L. Hanzo, "Joint radar and communication design: Applications, state-of-the-art, and the road ahead," *IEEE Trans. Commun.*, vol. 68, no. 6, pp. 3834–3862, Jun. 2020.
[52] R. Zhang et al., "Integrated sensing and communication with massive MIMO: A unified tensor approach for channel and target parameter estimation," *IEEE Trans. Wireless Commun.*, vol. 23, no. 8, pp. 8571–8587, Aug. 2024.
[53] F. Liu, W. Yuan, C. Masouros, and J. Yuan, "Radar-assisted predictive beamforming for vehicular links: Communication served by sensing," *IEEE Trans. Wireless Commun.*, vol. 19, no. 11, pp. 7704–7719, Nov. 2020.
[54] S. Huang, M. Zhang, Y. Gao, and Z. Feng, "MIMO radar aided mmwave time-varying channel estimation in MU-MIMO V2X communications," *IEEE Trans. Wireless Commun.*, vol. 20, no. 11, pp. 7581–7594, Nov. 2021.
[55] Z. Gao et al., "Integrated sensing and communication with mmWave massive MIMO: A compressed sampling perspective," *IEEE Trans. Wireless Commun.*, vol. 22, no. 3, pp. 1745–1762, Mar. 2023.
[56] C. B. Barneto, S. D. Liyanaarachchi, M. Heino, T. Riihonen, and M. Valkama, "Full duplex radio/radar technology: The enabler for advanced joint communication and sensing," *IEEE Wireless Commun.*, vol. 28, no. 1, pp. 82–88, Feb. 2021.
[57] C. Han and Y. Chen, "Propagation modeling for wireless communications in the terahertz band," *IEEE Commun. Mag.*, vol. 56, no. 6, pp. 96–101, Jun. 2018.
[58] Y. Ma et al., "Time-modulated arrays in scanning mode using wideband signals for range-Doppler estimation with time-frequency filtering and fusion," *IEEE Trans. Aerosp. Election. Syst.*, vol. 60, no. 1, pp. 980–990, Feb. 2024.
[59] L. Cheng, Y.-C. Wu, and H. V. Poor, "Probabilistic tensor canonical polyadic decomposition with orthogonal factors," *IEEE Trans. Signal Process.*, vol. 65, no. 3, pp. 663–676, Feb. 2017.
[60] R. Zhang et al., "Channel estimation for movable-antenna MIMO systems via tensor decomposition," *IEEE Wireless Commun. Lett.*, early access, Aug. 29, 2024, doi: 10.1109/LWC.2024.3450592.
[61] M. Sørensen and L. De Lathauwer, "Blind signal separation via tensor decomposition with Vandermonde factor: Canonical polyadic decomposition," *IEEE Trans. Signal Process.*, vol. 61, no. 22, pp. 5507–5519, Nov. 2013.
[62] S. M. Kay, *Fundamentals of Statistical Signal Processing*. Englewood Cliffs, NJ, USA: Prentice-Hall PTR, 1993.
[63] X. Liu and N. D. Sidiropoulos, "Cramer–Rao lower bounds for low-rank decomposition of multidimensional arrays," *IEEE Trans. Signal Process.*, vol. 49, no. 9, pp. 2074–2086, Sep. 2001.

Ruoyu Zhang (Member, IEEE) received the B.E. and Ph.D. degrees in information and communication engineering from Harbin Institute of Technology, Harbin, China, in 2014 and 2019, respectively.

From 2017 to 2018, he was a visiting student with the Department of Electrical and Computer Engineering, The University of British Columbia, Vancouver, BC, Canada. He is currently an Associate Professor with the School of Electronic and Optical Engineering, Nanjing University of Science and Technology, Nanjing, China. His research interests include integrated sensing and communication, massive MIMO, millimeter-wave communications, and sparse signal processing.

Xiaopeng Wu received the B.E. degree in electronic engineering from Nanjing University of Science and Technology, Nanjing, China, in 2023, where he is currently pursuing the M.S. degree with the School of Electronic and Optical Engineering.

His current research interests include the target detection and signal processing on integrated sensing and communication.

Yi Lou (Member, IEEE) received the B.S. degree in communication engineering from Jilin University, Changchun, Jilin, China, in 2009, and the M.S. and Ph.D. degrees in communication engineering from Harbin Institute of Technology, Harbin, China, in 2013 and 2017, respectively.

He was a visiting student with The University of British Columbia, Kelowna, BC, Canada, in 2016. From 2018 to 2022, he was an Associate Professor with Harbin Engineering University, Harbin. Since 2022, he has been an Associate Professor with the College of Information Science and Engineering, Harbin Institute of Technology (Weihai), Weihai, China. His research interests include underwater communications and cooperative communications.

Dr. Lou received the Best Poster Award from ACM WUWNet 2021.

Feng-Gang Yan received the B.E. degree in information and communication engineering from Xi'an Jiaotong University, Xi'an, China, in 2005, the M.S. degree in information and communication engineering from the Graduate School of Chinese Science of Academic, Beijing, China, in 2008, and the Ph.D. degree in information and communication engineering from Harbin Institute of Technology (HIT), Harbin, China, in 2014.

From July 2008 to March 2011, he was a Research Associate with the Fifth Research Institute of China Aerospace Science and Technology Corporation, Beijing, where his research was mainly focused on remote sensing image processing. Since 2020, he has been a Professor with the School of Information Science and Engineering, HIT (Weihai), Weihai, China. During the past ten years, he has authored and co-authored more than 80 publications, mainly on IEEE journals. His current research interests include array signal processing, radar polarimetry, and electronic countermeasures.

Dr. Yan was awarded The Excellent Young Scientists Fund of the Natural Science Foundation of Shandong Province and the Taishan Scholar Special Funding Project.

Zhiquan Zhou received the M.S. and Ph.D. degrees in information and communication engineering from Harbin Institute of Technology, Harbin, China, in 1998 and 2004, respectively.

He was an Associate Professor from 2005 to 2011 and has been a Professor with the School of Information Science and Technology, Harbin Institute of Technology (Weihai), Weihai, China, since 2011. His current research focuses on sensor design and signal processing, ocean surveillance, and communication systems.

Wen Wu (Senior Member, IEEE) received the Ph.D. degree in electromagnetic field and microwave technology from Southeast University, Nanjing, China, in 1997.

He is currently a Professor with the School of Electronic Engineering and Optoelectronic Technology, Nanjing University of Science and Technology, Nanjing, where he is also the Associate Director of the Ministerial Key Laboratory of JGMT. He has authored or co-authored more than 60 journal articles and conference papers. He has submitted five patent applications. His current research interests include microwave and millimeter-wave theories and technologies, microwave and millimeter-wave detection, and multimode compound detection.

Dr. Wu was a recipient of the Ministerial- and Provincial-Level Science and Technology Awards six times.

Chau Yuen (Fellow, IEEE) received the B.Eng. and Ph.D. degrees from Nanyang Technological University, Singapore, in 2000 and 2004, respectively.

He was a Postdoctoral Fellow with Lucent Technologies Bell Labs, Murray Hill, NJ, USA, in 2005. From 2006 to 2010, he was with the Institute for Infocomm Research, Singapore. From 2010 to 2023, he was with the Engineering Product Development Pillar, Singapore University of Technology and Design, Singapore. Since 2023, he has been with the School of Electrical and Electronic Engineering, Nanyang Technological University, where he is currently the Provost's Chair of Wireless Communications and an Assistant Dean of Graduate College. He has four U.S. patents and published over 400 research papers at international journals.

Dr. Yuen received the IEEE Communications Society Leonard G. Abraham Prize in 2024, the IEEE Communications Society Best Tutorial Paper Award in 2024, the IEEE Communications Society Fred W. Ellersick Prize in 2023, the IEEE Marconi Prize Paper Award in Wireless Communications in 2021, the IEEE APB Outstanding Paper Award in 2023, and the EURASIP Best Paper Award for Journal on Wireless Communications and Networking in 2021. He currently serves as an Editor-in-Chief for *Springer Nature Computer Science* and an Editor for IEEE TRANSACTIONS ON VEHICULAR TECHNOLOGY, IEEE SYSTEMS JOURNAL, and IEEE TRANSACTIONS ON NETWORK SCIENCE AND ENGINEERING, where he was awarded as the IEEE TNSE Excellent Editor Award and the Top Associate Editor for TVT from 2009 to 2015. He also served as the Guest Editor for several special issues, including IEEE JOURNAL ON SELECTED AREAS IN COMMUNICATIONS, *IEEE Wireless Communications Magazine*, *IEEE Communications Magazine*, *IEEE Vehicular Technology Magazine*, IEEE TRANSACTIONS ON COGNITIVE COMMUNICATIONS AND NETWORKING, and *Applied Energy* (Elsevier). He is a Distinguished Lecturer of the IEEE Vehicular Technology Society, Top 2% Scientists by Stanford University, and also a Highly Cited Researcher by Clarivate Web of Science.